Lane Preference in a Simple Traffic Model

Justin Krometis

Thesis submitted to the faculty of the Virginia Polytechnic Institute and State University in partial fulfillment of the requirements for the degree of

Master of Science
In
Mathematics

George Hagedorn, Chair
Beate Schmittmann
Royce K. P. Zia

April 23, 2004
Blacksburg, Virginia

Keywords: driven lattice gas, Monte Carlo simulations, non-equilibrium steady-state, phase transition, highway traffic

Lane Preference in a Simple Traffic Model

Justin Krometis

(ABSTRACT)

We examine the effect of lane preference on a quasi one-dimensional three-state driven lattice gas, consisting of holes and positive and negative particles, and periodic boundary conditions in the longitudinal direction. Particles move via particle-hole and, with a lesser rate, particle-particle exchanges; the species are driven in opposite directions along the lattice, each preferring one of the lanes with a given probability, p. The model can be interpreted as traffic flow on a two-lane beltway, with fast cars preferring the left lane and slow cars preferring the right, viewed in a comoving frame. In steady-sate, the system typically exhibits a macroscopic cluster containing a majority of the particles. At very high values of p, a first order transition takes the system to a spatially disordered state. Using Monte Carlo simulations to analyze the system, we find that the size of the cluster increases with lane preference. We also observe a region of negative response, where increasing the lane preference *decreases* the number of particles in their favored lane, against all expectations. In addition, simulations show an intriguing sequence of density profiles for the two species. We apply mean-field theory, continuity equations, and symmetries to derive relationships between observables to make a number of predictions verified by the Monte Carlo data.

This research was funded by Virginia Tech Mathematics departmental funds and National Science Foundation grant DMR-0088451.

To the three special ladies in my life: Leigh-Anne, Anne, and Mom

Acknowledgments

First and foremost, I would like to thank Beate Schmittmann for accepting the day I walked into her office and proposed that we start a project together, and for the countless hours we spent pondering, writing, editing, and conversing. She has been an excellent mentor but most of all a good friend.

I also want to thank George Hagedorn and Royce Zia for their always friendly and easy-going manner, and also for their assistance in the completion of this project.

I am deeply indebted to all of the graduate students in 465 McBryde for their support during my time in the graduate school. In particular, I want to acknowledge John Singler for his help in learning LaTeX, and Sharon Hughes for her support and friendship throughout the ups and downs of teaching and classes, and her selflessness on one particularly long Friday afternoon.

I owe many more thanks to those in the Math Department: to Peter Haskell for advice throughout my time here and going forward, to Ken Hinson for his work on the servers that I used so exhaustively and tolerance of my inexperience with them, to Hannah Swiger for her aid in maneuvering through the bureaucratic maze of graduate school, and to Eileen Shugart for the assistance, advice, programs, and friendship that she provides to all math graduate students.

I am grateful to Don Langrehr for his support and advice, for showing me a new way of looking at the world, and for all the fun times shaking things up in town.

My time at Virginia Tech was not without its personal struggles, and I would like to recognize those who helped me through the most difficult of them, including Mike, Colleen, Katrin, Jane ($\times 2$), Kristin, Rick, and many others too numerous to name. Their support and dedication during my time of need will stay with me always.

I want to express much love and many thanks to my family - Anne, James, Damon, Dad, Lynn, Kurt, and everyone else - for just generally being wonderful and there for me.

Lastly, I want to thank Leigh-Anne for being a compassionate and supportive partner through all of this. The entire process was infinitely more rewarding for sharing it with such a talented individual, and I cannot imagine having completed it otherwise.

Contents

List of Figures

List of Tables

1 Introduction

Thermal equilibrium has been well-studied in physics and mathematics over the last century. Most of the associated concepts and techniques have been successfully used for decades. As an example, let us consider one classic equilibrium system, an ideal gas exposed to a gravitational field and confined in a cylinder of infinite height, at constant temperature. In this case, the particle density as a function of height is given by the barometric height formula, obtained from the canonical distribution. The system has all of the hallmark traits of an equilibrium state. There are no net mass currents; each particle moving to a new height is just as likely to be replaced by one making the opposite change. The particles can be assigned a potential energy based on their position, namely $V(h) = mgh$. The system undergoes constant microscopic fluctuations, but the macroscopic variables, such as particle density, are time-independent.

But do these traits define equilibrium? A steady-state is a condition where microscopic, time-dependent fluctuations may occur in a system but all macroscopic variables have reached stationary values. Are all steady-states equilbrium states? Or are there *non-equilibrium* steady states? Before answering this question, we present a second example.

Imagine a glass of water heated on the left by a light source. The liquid on the left is warmed by the light, expands, and consequently rises to the surface. Water at the bottom of the glass moves to fill the void left by the heated water, becomes heated itself, and rises. Thus we have a continuous clockwise mass current of water in the glass. Notice that any two snapshots of the system taken at widely different times will look the same at the macroscopic level - mass densities, currents, pressue gradients, and any other variable will be identical, indicating that this is a steady-state. In addition, no potential energy can be assigned to describe the motion; molecules are driven in directions dictated by their position in the system only to arrive in the same position once more. Here we clearly have a different sort of steady state than in the example above. We will now use the framework of statistical mechanics to put these distinctions in mathematical terms.

Every statistical system is characterized by a set of possible configurations, along with dynamics that define rates with which each of those configurations C evolves into another, C': $W[C \to C']$. The rate of change of the probability that the system is in a given configuration is then given by what is known as the "master equation":

$$\partial_t P(C) = \sum_{C'} \{P(C')W[C' \to C] - P(C)W[C \to C']\} \tag{1.1}$$

Note that this equation states conservation of probability. Also, the term inside the $\{\cdot\}$ is the net probability current from C' to C. Recall that there are no non-zero net mass currents in our example of an equilibrium state, the ideal gas subject to gravity. A different, but related property that it exhibits is that all net probability currents are 0 - that each configuration C is equally likely to evolve into another configuration C' as vice versa. Notice

that this is equivalent to setting each individual term inside the summation to 0. This condition, known as detailed balance, is how we define equilibrium in mathematical terms.

In a steady-state, however, we only require that the probability distribution of the system is time-independent. In other words, the derivative on the left in equation (1.1) is 0 for all C. Notice that this condition is much less restrictive than that of detailed balance; there should be many non-equilibrium steady-states (denoted NESS)!

We have said that NESSes have non-zero net flows between two configurations, and yet have time-independent macroscopic variables. In our example system, a cup of water exposed to a light source, one configuration (call it C) evolves into others where the molecules near the source have risen. However, this flow of probability out of (C) is balanced by an incoming current from other configurations where particles near the source are nearer to the base of the cup. This is an example of a more general characteristic of a NESS: current "loops" in configuration space.

Because they have fewer constraints than equilibrium systems, non-equilbrium steady-states are much more difficult to classify. It is therefore no surprise that relatively little is known about them compared to equilibrium steady states. Much work has recently been done on simple models that exhibit NESSes in an effort to better understand them. A group of these models particularly relevant to this thesis is the driven diffusive system, in which particles on a lattice are exposed to a driving force. We will now focus our attention on work in this field.

The "standard model" of driven diffusive systems was introduced by Katz, et al [1] in 1983. It consists of an Ising lattice gas exposed to a driving field. Particles interact via the usual nearest-neighbor Ising attraction and jump to nearest-neighbor empty sites, subject to the local energetics and biased by the driving field. Periodic boundary conditions (PBC) are imposed in the direction of the lattice. Under these conditions, the particles tend to move along the direction of the field. While the modelling of fast ionic conductors and other physical systems provided motivation for this study, the primary goal was to explore far from equilibrium systems in one of their more simple examples.

Following this lead, many such systems have been studied in the subsequent two decades. The typical model is a variation on the standard model, where changes are made in system-size, shape, filling fraction, particle interactions (repulsion or attraction), or types of particles. A natural extension of these models is a two-species diffusion process, where "positive" and "negative" particles are driven in opposite directions across a lattice, mediated by a background of holes [2]. Even in the absence of inter-particle attractions, these systems can exhibit phase transitions as the diffusing particles of each species disrupt or "block" the movement of the other. At low densities or driving fields, the system is typically in a disordered phase, where the particles move relatively freely past one another and all local densities are spatially uniform. At higher densities or fields, an ordered phase emerges, consisting of a single blockage containing the majority of the particles and a sparsely populated "traveler" region where those that trickle out of the cluster move quickly through this region

to end up on the other end of the block.

A particularly relevant example of this kind consists of an $L \times L$ lattice with three states (+,-,0), with equal numbers of positive and negative particles [3]. The particles interact solely through an excluded volume constraint, i.e., each lattice site may not contain more than one particle. There are two basic dynamic processes: particles may exchange with nearest-neighbor holes (known as particle-hole exchanges, or PHE) and particles of opposite charge are allowed to exchange positions with a smaller probability (particle-particle exchange, PPE). This system appears to undergo a phase transition between homogeneous (disordered) and phase-separated (ordered) states that depends on filling fraction, magnitude of the driving field, and likelihood of PPE [3].

In recent years, researchers have sought to examine two-species systems on still simpler lattices in an effort to get better understanding of the phase transitions that are often observed in these systems. In particular, studies have been conducted on two-species diffusion in one-dimensional $(1 \times L)$ and quasi one-dimensional $(2 \times L)$ lattices. In the one-dimensional equivalent of the system described above, an exact solution for the stationary state has been found [4]. It demonstrates that numerous small clusters form and prevent long-range order (LRO) - a single cluster containing most of the particles - from occuring, and thus that no phase transition from the disordered phase exists [4].

One might expect that adding a second lane to the system would allow particles to move past one another more freely, serving to simply increase the likelihood of particle-particle exchange and yet leaving general features of the 1-D model intact. However, Monte Carlo (MC) simulations of the $2 \times L$ system by Korniss, et al [5], where the PHE rate is ten times higher than the PPE rate, appear to show a phase transition between disorder and LRO similar to that found in the $(L \times L)$ lattice. Monte Carlo data and analytical arguments indicate that the ratio of the average cluster size l_0 and the system size is independent of the latter: $l_0/L = 0.472$. Lastly, they provide evidence that as $L \to \infty$, the cluster size distribution around l_0 appears to approach a Gaussian. Each of these results implies that the phase transition will continue to exist for all system sizes. Recent analytical work, on the other hand, conjectures that the apparent transition is a finite-size effect and ceases to exist for large but finite L [6]. Neither position has been definitively disproved.

Systems such as those above can be interpreted in a particularly intuitive way as highly-simplified models of traffic [7] on a one- or two-lane loop road or beltway traversed by "fast" (positive particles) and "slow" cars (negative particles). If the loop is observed in a frame rotating at the average of the two velocities, the fast cars appear to be moving in one direction while the slow move in the opposite direction, and we recognize our system dynamics. Because the clusters are moving along with the rotating frame, ordering is probably best viewed not as formation of "traffic jams" in the traditional sense, but as moving clusters of cars with the slow cars trapping the fast cars at the front and the fast trapping the slow at the rear.

The intent of our work is to investigate the effect of exposing the particles to a potential

across the lanes in a two-lane loop road. In the traffic analogy, this is equivalent to making the fast cars prefer the left lane and slow cars prefer the right lane, as is often the case on real highways. In this system, as we will see, it is largely the cars in unfavored lanes that cause blockages, behavior that is, in practice, typical of cars on two-lane highways.

In this thesis, we will focus primarily on how increasing this transverse bias causes the system to deviate from the symmetric case studied in [5]. Our expectations were that adding a lane preference would decrease the interference of the traffic and, consequently, the jamming. However, we will show that it actually results in a *more* ordered system or, in other words, increases the strength of the blockages in the traffic. We also unexpectedly observe parameter regions where increasing the transverse bias increases the probability of finding particles in their unfavored lane. In some cases, the more the fast cars prefer the left lane, the more they end up in the right!

The thesis is organized as follows: We will begin by defining the parameters and dynamics of the model. Then we will outline the results obtained from Monte Carlo simulations, including those above. The results we obtained by integration of Mean-Field (MF) theory equations of motion will then be presented, followed by analytical results we obtained from conservation laws and MF approximations. Lastly, we will conclude with some questions and suggestions regarding further related research.

2 Model

Our system exists on a $2 \times L$ lattice with periodic boundary conditions in the longitudinal direction. Sites are denoted by (x, y) where $0 \leq x \leq L-1$ and $y = 0, 1$. Each cell in the lattice can be occupied by a hole (0, "unoccupied") or either a positive (+) or negative (−) particle. Our system is limited by an excluded volume constraint, i.e. no site (x, y) can be occupied by more than one particle at a time. We define a local charge variable $q(x, y)$ as 1 (-1) if the site (x, y) is occupied by a positive (negative) particle and 0 if it is unoccupied, and a local mass $m(x, y) = |q(x, y)|$. The system is neutral ($\sum_{x,y} q(x, y) = 0$) and half-filled ($\sum_{x,y} m(x, y) = L$); we define $N = \frac{1}{2}L$ to be the number of particles of each type in the system. Particles on the lattice are exposed to infinite "electric" field along the system which drives each species of particles in opposite directions; jumps against it are forbidden. We also impose a bias across the "lanes" characterized by the variable b, which is zero when no bias is imposed across the lanes and unity for a perfect lane bias. In addition to these constraints, positive and negative particles are allowed to exchange position - referred to as "charge exchange" - with rate $\gamma = 0.1$.

In our Monte Carlo simulations, we choose a particle at random (site (x, y)) and then select a neighboring site (x', y'). We define $\delta x = x' - x$ and $\delta y = y' - y$. Exchange probabilities are as follows:

(a) If $\delta y = 0$, and $m(x', y') = 0$

$$W_{phx} = \left\{ \begin{array}{c} 1 \text{ if } q(x, y) \cdot \delta x = 1 \\ 0 \text{ if } q(x, y) \cdot \delta x = -1 \end{array} \right\} \tag{2.1a}$$

(b) If $\delta y = 0$, and $m(x', y') = 1$

$$W_{ppx} = \left\{ \begin{array}{c} \gamma \text{ if } q(x, y) \cdot \delta x = 1 \\ 0 \text{ if } q(x, y) \cdot \delta x = -1 \end{array} \right\} \tag{2.1b}$$

(c) If $\delta x = 0$, and $m(x', y') = 0$

$$W_{phy} = \left\{ \begin{array}{c} 1 \text{ if } q(x, y) \cdot \delta y = 1 \\ 1 - b \text{ if } q(x, y) \cdot \delta y = -1 \end{array} \right\} \tag{2.1c}$$

(d) If $\delta x = 0$, and $m(x', y') = 1$

$$W_{ppy} = \left\{ \begin{array}{c} \gamma \text{ if } q(x, y) \cdot \delta y = 1 \\ \gamma(1 - b) \text{ if } q(x, y) \cdot \delta y = -1 \end{array} \right\} \tag{2.1d}$$

If the exchange probability is 1, the exchange is simply performed. Exchanges between particles of the same charge are ignored. Note that positive/negative particles "prefer" lane 1/0, and that the strength of this preference varies with b. Also, note the following:

Symmetry 1 *The dynamics of the system are unchanged if the following three exchanges are made:*

$$x \to L - x - 1$$
$$y \to 1 - y$$
$$q \to -q$$

The latter is the exchange of particle species.

We define one Monte Carlo step (MCS) to be the selection of $2N$ particles. Our simulations varied from $L = 10^2$ to 10^4 and in length from 5×10^5 to 10^7 MCS. Measurements were usually taken every 100 MCS, though occasionally longer simulations warranted that this spacing be increased to 1000. Unless otherwise stated, all measured quantities are time averages taken after the steady-state has been reached.

To characterize ordered and disordered states, we first define the magnitude of the Fourier transform of the local mass $m(x, y)$:

$$\tilde{m}_{sys} = \left| \frac{1}{2L} \sum_{y=0}^{1} \sum_{x=0}^{L-1} e^{i2\pi x/L} m(x, y) \right| \tag{2.2a}$$

$$\tilde{m}_{y} = \left| \frac{1}{L} \sum_{x=0}^{L-1} e^{i2\pi x/L} m(x, y) \right|, \; y = 0, 1 \tag{2.2b}$$

Note that these reach their maximum value for a "fully-ordered" cluster where, for instance, a site (x, y) contains a particle if and only if $0 \leq x \leq L/2 - 1$,

$$\tilde{m}_{sys} = \tilde{m}_0 = \tilde{m}_1 = \left| \frac{1}{L} \sum_{x=0}^{L/2-1} e^{i2\pi x/L} \right| = \frac{1}{L \sin(\pi/L)} \overset{L\to\infty}{\longrightarrow} \frac{1}{\pi} \approx 0.318 \tag{2.3}$$

Also, they reach their minimum value, 0, for a "fully-disordered" cluster where particles are evenly spaced throughout the system, e.g., $m(x, y) = 1$ for x even and $m(x, y) = 0$ for x odd.

To make some sense of the complicated formula for $\tilde{m}_{sys}$, we consider the complex plane, where each $e^{i2\pi x/L}$ term represents a unit vector making an angle of $2\pi x/L$ with the real axis. Thus, the order parameter is equivalent to summing over all of these vectors (weighted by the number of particles at the corresponding x) and taking the magnitude of the resultant. Thus, we see that in a disordered system, the vectors would be in a variety of directions, so the resultant would have near-zero magnitude. In an ordered system, the vectors would be pointing in a particular direction - limited by the excluded-volume constraint - and thus would have a resultant with a distinctly non-zero modulus. Note, however, that $\tilde{m}_{sys}$ is not sensitive to the charge of the particles - it is merely a measure of how clustered they are.

We use $\tilde{m}_{sys}$ to distinguish between ordered and disordered states in our simulations. We determine that the system is in an ordered steady state if $\tilde{m}_{sys}$ is above a certain value and fluctuations were within a certain threshold. Averages for ordered configurations are taken over the last "string" of data points that met this criteria. In other words, when this criteria is violated, we discard our averages and start anew. The typical number of MCS that the system requires before reaching steady-state is about 2×10^5 for $L = 1000$; this time is shorter for smaller system-sizes and longer for larger ones.

Now we introduce three associated order parameters to characterize the order of a steady state, the first of which is used in the study of the symmetric $2 \times L$ system [5]:

$$\Omega_{sys} = \langle \tilde{m}_{sys} \rangle \tag{2.4a}$$

$$\Omega_y = \langle \tilde{m}_y \rangle \, , \, y = 0, 1 \tag{2.4b}$$

Here and in the remainder of the thesis, we use $\langle \cdot \rangle$ to denote an average over the steady-state configurations of a run. Obviously, each of these observables also attains a maximum value of ≈ 0.318 for a system that stays perfectly ordered through the entire run. For a disordered system where particles are scattered randomly throughout the system, $\Omega_{sys} = \Omega_0 = \Omega_1 = 0$ up to a finite size effect of $1/\sqrt{L}$. Note that for a typical cluster, the mass densities in each lane will also be roughly similar, so these three variables are usually approximately equal. Thus, we will typically refer to Ω_{sys} as the "order parameter."

We said that $\tilde{m}_{sys}$ is the magnitude of a vector in the complex plane, but the angle ϕ that the vector makes with the real axis is also useful as it specifies the center of mass of the system: $x_0 = L\phi/2\pi$. This is calculated by

$$\phi = arctan(Im(z)/Re(z)), \text{where } z = \frac{1}{2L} \sum_{y=0}^{1} \sum_{x=0}^{L-1} e^{i2\pi x/L} m(x, y) \tag{2.5}$$

This variable is used to recenter profiles (variables that depend on x) that are measured in simulations. Because of the periodic boundary conditions, the macroscopic cluster, and thus the center of mass, forms at an arbitrary position in each simulation. To standardize our profiles before averaging, we shift them so that the center of mass is at $L/2$. This explains the fact that profiles given later in Figures 3.1, 3.6, and others show clusters centered roughly at $x_0 = L/2$.

3 Monte Carlo Results

3.1 Typical System Configuration

At a given time, the system typically is typically found in one of two phases: "ordered" or "disordered." A perfect disordered phase would consist of particles scattered completely randomly throughout the system, so that a time-averaged mass profile is spatially uniform throughout the system. While the disordered phases of this model show some microscopic clustering, they usually approximate this idealization very well. Note that in this scenario, we expect - and, in later sections, find - that each lane contains the vast majority of its favored species of particle.

In a perfectly ordered configuration, all of the particles in the system are contained in a single cluster devoid of holes. In practice, however, ordered phases exhibit, at any particular time, a small percentage (dependent on b and γ) of the particles which are outside of the cluster, moving relatively freely from one end of the cluster around the ring to the other end of the cluster. We will refer to this region as the "traveler region." Its existence can be seen in Figure 3.1, a time-averaged mass profile of a typical ordered system configuration, where we see the cluster as a section of large mass densities, and the traveler region as the remainder of the system exhibiting a near-zero average mass.

Now that we have discussed the typical configurations of the two phases, we will examine how the system makes the transition between them.

3.2 Phase Transition

In Figure 3.2, we see Monte Carlo results for the dependence of Ω_{sys} on the cross-lane bias, b, and the system size, L. Note that the system stays in an ordered state ($\Omega_{sys} \approx 0.3$) for all but extremely strong biases, after which we see a sharp drop to a disordered state ($\Omega_{sys} \approx 0$). While the dramatic drop in the order parameter appears to be characteristic of a first-order transition, we further analyzed the behavior via a hysteresis loop. Beginning with a perfect transverse bias ($b = 1$), we decreased b in intervals of 0.001, using the final configuration from the previous step as the initialization for the succeeding one and simulating 10^5 MCS at each value, until we reached $b = 0.95$, and then returned to 1 in a similar fashion. Figure 3.3, which contains plots of Ω_{sys} for the loop, shows a distinct hysteresis effect indicating a first-order phase transition.

Another feature characteristic of a first order transition in a finite system is repeated "switching" from one phase to the other. An example of this phenomenon can be found in Figure 3.4, which shows a time-trace of such a system. These anomalous states were found at biases near the transition between ordered and disordered states, and were only observed for small system sizes. For $L = 100$ the characteristic life time of each state was on the order of 10^5 MCS, but increased to $\approx 10^7$ for $L = 250$. So, in principle, larger (but finite) systems

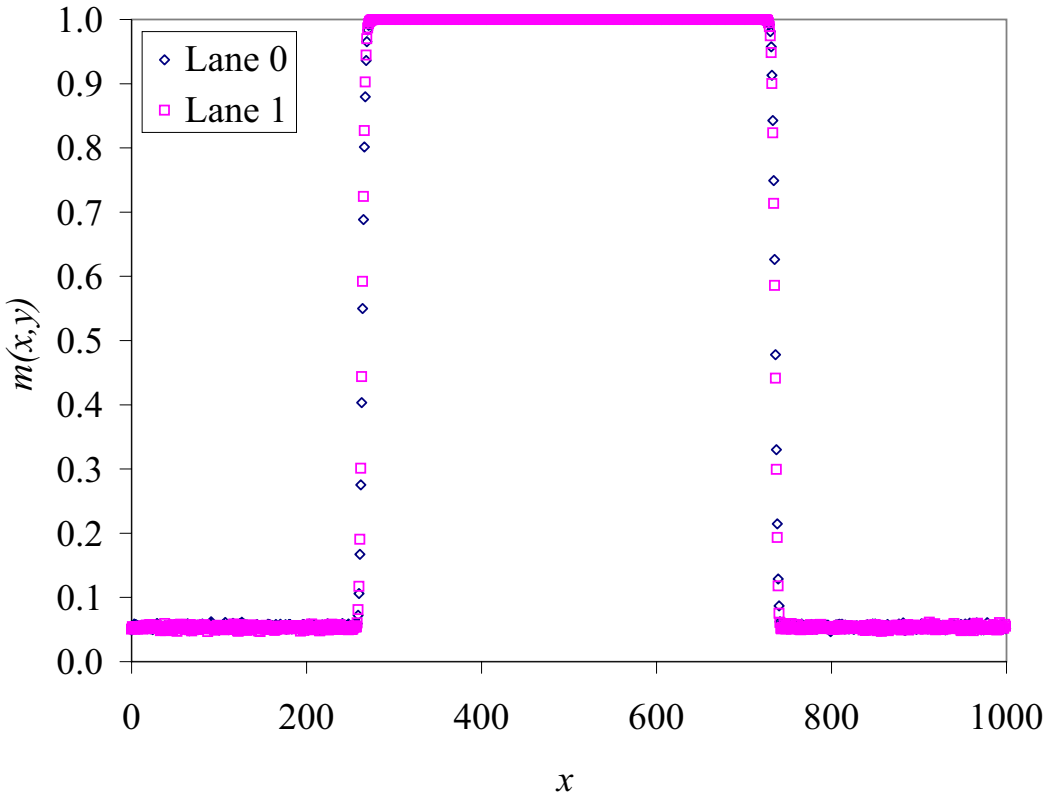

Figure 3.1: Typical mass profile for ordered phase

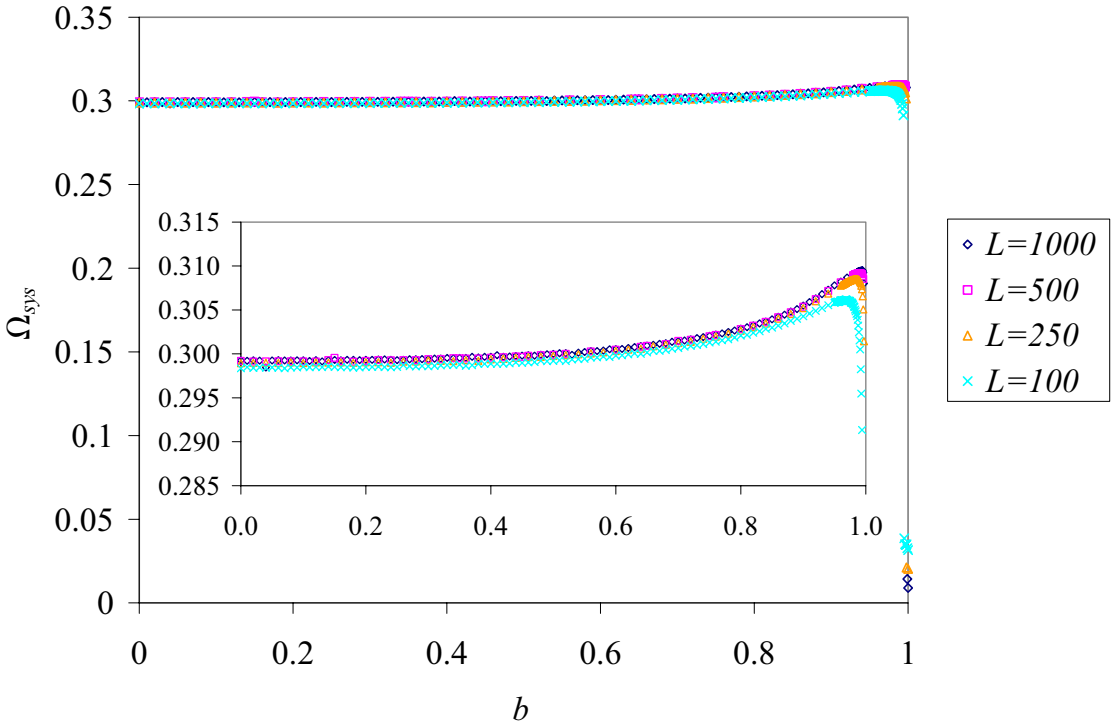

Figure 3.2: Steady-state Ω_{sys} vs. b, L; Inset: Close-up of curve for ordered phases

may also exhibit switching between phases but on time scales that were unattainable in our simulations.

In the next section, we will take a closer look at Figure 3.2, the dependence of the order parameter on b.

3.3 Order Parameter

As noted in equation (2.3), the order parameter (Ω_{sys}) reaches a maximum value (≈ 0.318) for the perfectly ordered system. In Section 3.5, we show that this order parameter decreases uniformly as more particles escape the cluster and the mass density of the traveler region increases. One might expect that as the bias across the lane increases, fewer particles would be found in the "wrong" lane. As a result, flow of particles in the "correct" lane would be less impeded, the density of the traveler region increased, and the order parameter decreased. In other words, we expect that the more cars favor lanes, the less they interfere with each other, and therefore the more freely they move. However, in Figure 3.2, we see that through the majority of the ordered phase ($0 \leq b \lesssim 0.995$), the order parameter increases monotonically with the bias across the lanes. Shockingly, the bias increases the blocking! So we have

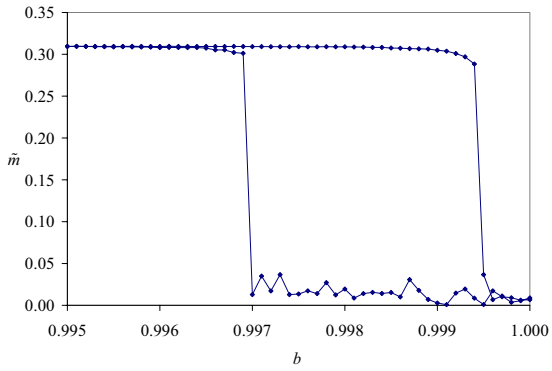

Figure 3.3: Hysteresis loop results: $\tilde{m}_{sys}$ vs. b

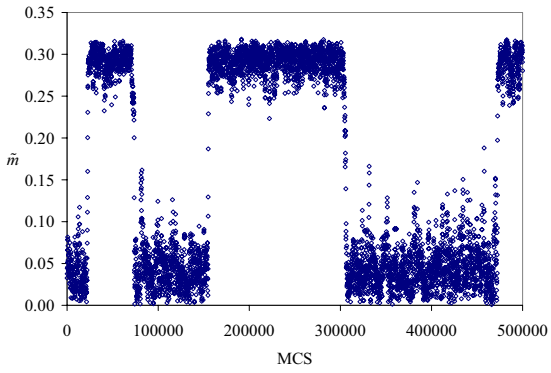

Figure 3.4: Time-trace of $\tilde{m}_{sys}$ for "switching" state at $L = 100$, $b = 0.994$

the surprising result that, on a two-lane ring road, as we increase the lane preference, the percentage of cars confined to the moving jam increases.

It is now natural to ask how b affects the internal composition of the cluster. In particular, how does it change the likelihood of finding each particle in its favored lane? We will answer this question in the next section.

3.4 Charge

We begin this section by defining the total charge in lane 1, which is given by

$$Q_1 = \left\langle \frac{2}{L} \sum_x q(x,1) \right\rangle \tag{3.1}$$

Note that by the definition of $q(x,1)$, Q_1 is a measure of how much more likely we are to find fast cars in the left lane than the right lane. It seems a reasonable assumption that increasing the lane preference of the cars will increase the likelihood that we find cars in their favored lane. In other words, the more a fast car favors the left lane, we expect to find it in that lane with greater probability. Figure 3.5 shows steady-state values for Q_1 as they depend on the lane preference, b. Note that the positive slope for $0 \leq b \lesssim 0.95$ indicates that our intuition is, for the most part, correct. However, we also note that there is a region of high transverse bias where $\partial_b Q_1 < 0$ and the system violates our reasoning. In particular, for this region, greater lane preference makes it less likely that we will find cars in their favored lanes!

To further probe this rather surprising result, we look at how the charge profile of the system changes with b. Figure 3.6 shows these profiles for a variety of biases and a system-size of 1000. The systems are centered so that $x = 500$ is the middle of the clusters in the two lanes. For $b = 0$, we see the tangent curve of the system with unbiased lanes [8]. As b

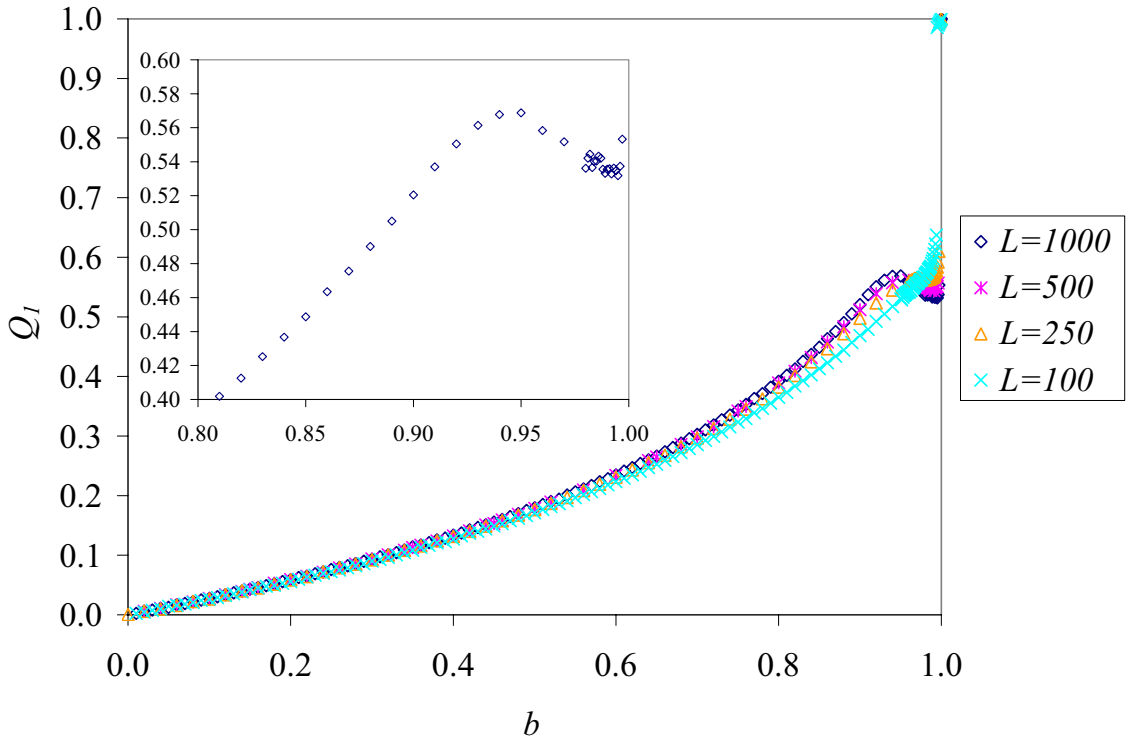

Figure 3.5: Steady-state Q_1 vs. b, L; Inset: High-b regime for $L = 1000$

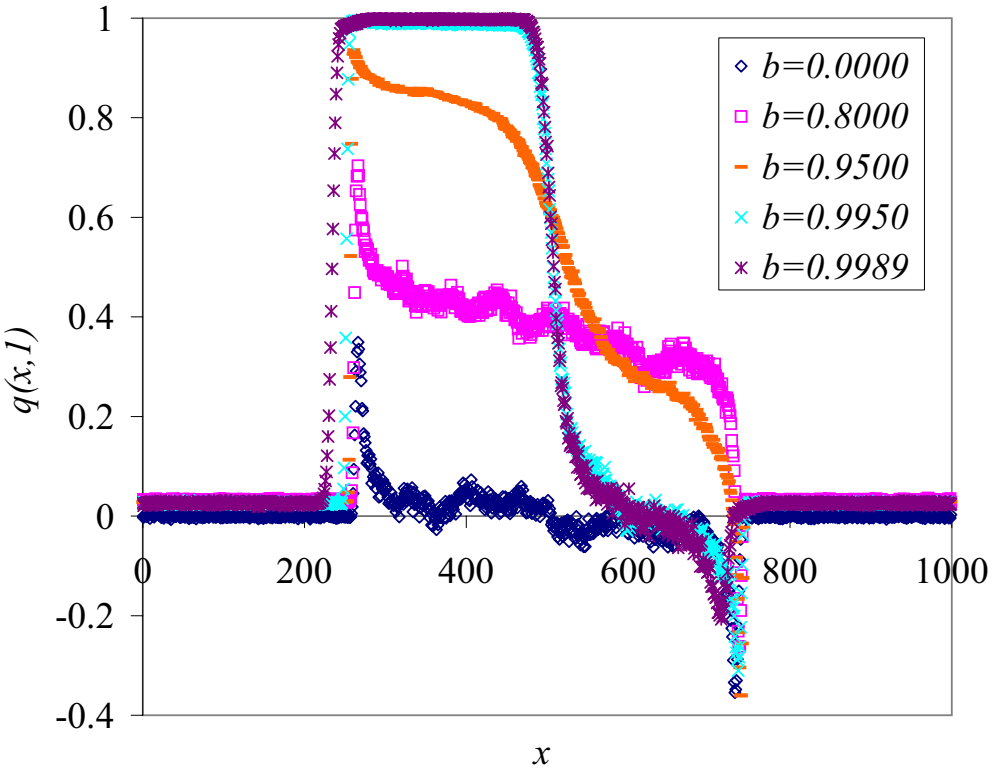

Figure 3.6: Charge profiles ($\langle q(x,1)\rangle$ vs. x) for various b's, $L = 1000$

increases to 0.8, the profile is still tangent-like, but shifted upwards by a constant. However, as b approaches 0.95, the maximum of the Q_1 vs. b graph, the shape of the profile changes as more positive (negative) particles move to the left (right) side of the cluster. The decrease in Q_1 appears to coincide with this "reordering" of the system. For the nearly perfect bias (0.995 or 0.9989), this effect is maximized and we see that the system develops three distinct sections: (1) the familiar traveler region, (2) a nearly charge-segregated or "favored" region, and (3) an approximately neutral or "mixed" region. Lastly, it is worth noticing that the systems with $b = 0.9989$ and $b = 0.995$ are very similar except that the first is offset from $x = 500$, indicating that for this system, the clusters in the two lanes are offset. This is an important feature of the system in the high-b limit; as the transverse bias approaches its critical value, the two lane clusters become more and more offset. Much information can be gleaned from this relatively simple form that the system takes for high b, but the analysis will be saved for Section 4.2.1.

While order and charge are two of the most prominent and easily interpreted features of a steady-state, other measurements can be just as valuable in interpreting the behavior of the

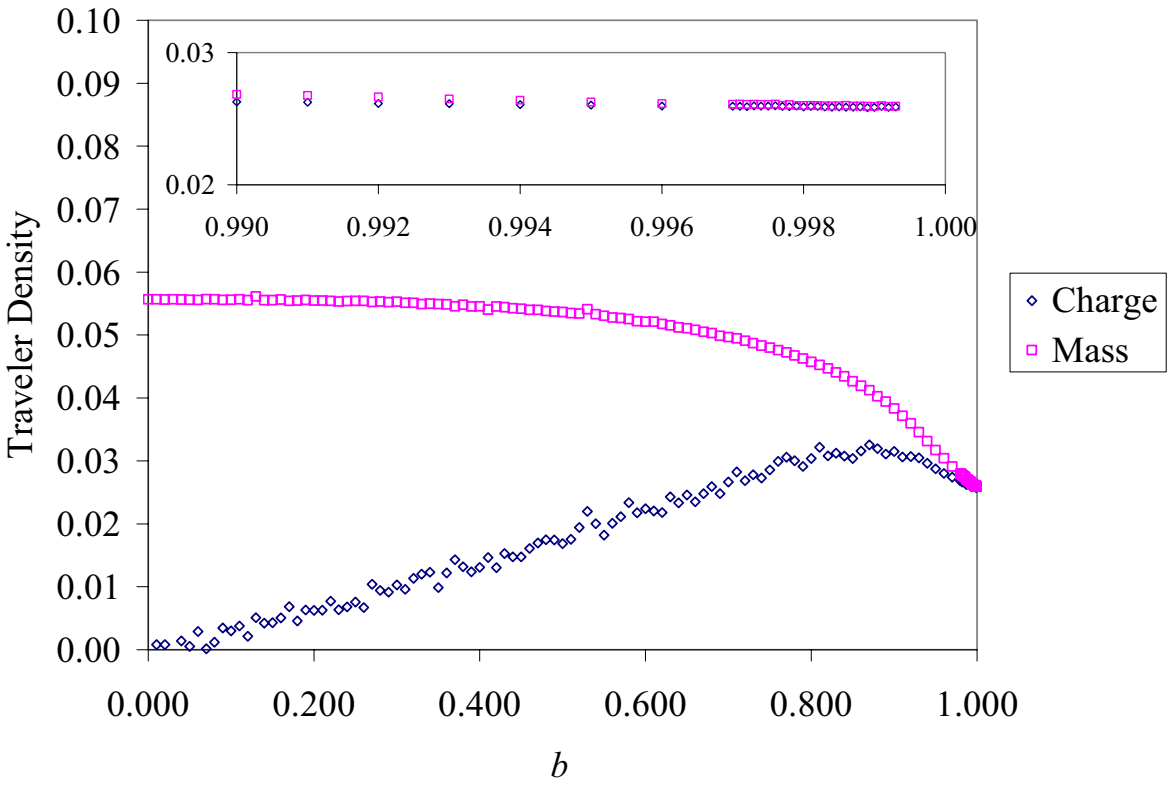

Figure 3.7: Steady-state m^*, q_1^* vs. b, $L = 1000$ for ordered configurations; Inset: Near transition

system. In the next section, we will look at an important one, the density of the travelers.

3.5 Traveler Region Densities

Recall that the traveler region is the sparsely populated portion of an ordered state, where the particles move rapidly from one end of the cluster to the other. We measured the mass and charge (in lane 1) densities for the traveler region of the steady state, averaged across the region and over the run (denoted m^* and q_1^*, respectively). Figure 3.7 plots these values vs. b at $L = 1000$. Plots for other system sizes were nearly identical.

A few features are worthy of attention. First, note that the charge density increases monotonically with b for much of the plot before decreasing and reaching the same value as the mass density as $b \to 1$. This maximum can be seen as a competing relationship between the increasing lane preference of particles in the traveler region and the decreasing mass density - the fewer the particles, the less charge to be found in the region. Note that the convergence of mass and charge density at $b \approx 1$ indicates that the traveler region is,

unsurprisingly, almost entirely charge segregated. In the inset, we see that both densities appear to be independent of b in the extreme high-b, but ordered, regime. Much information can be gleaned from this constant value, measured as ≈ 0.2595; this will be discussed at length in Section 4.2.1.

Lastly, note that the mass density in the traveler region decreases with transverse bias. Since the order parameter increases with b, we see that as m^* increases, Ω_{sys} does the opposite. This makes intuitive sense because the cluster is the complement of the traveler region; thus, if the number of travelers in the system grows, the cluster size and, consequently, Ω_{sys} must decrease. We will now solidify this conjecture mathematically.

To do so, we begin by assuming that the traveler region is uniformly dense ($m(x, y) = m^*$) and the cluster contains no holes ($m(x, y) = 1$). This assumption is justified by the approximately constant values seen in the mass profile, Figure 3.1. We then compute the order parameter directly via equation (2.4a). The computation is quite lengthy, so step-by-step calculations are left to Appendix A.1.

$$\Omega_{sys} = \frac{(1 - m^*) sin\left(\frac{\pi}{2(1-m^*)}\right)}{L sin\left(\frac{\pi}{L}\right)} \tag{3.2}$$

Figure 3.8 shows plots of measured values of Ω_{sys} as functions of m^* compared with those calculated from this equation using measured values of m^*. Data points from the disordered phase are uninteresting and therefore omitted; without blockages the entire system acts as a traveler region with $m^* \approx 1/2$ and $\Omega_{sys} \approx 0$, values which satisfy equation (3.2), albeit in an extreme case. The agreement between the two is excellent for much of the domain of m^*. Note the behavior at the left end of the curve as m^* approaches its high-b limit of 0.0256, where Ω_{sys} "dives" rapidly as a result of an increasing offset between the two lanes.

3.6 Cluster Size Distribution

Now that we have studied the steady-state traveler densities, we turn to a feature intimately related to them: the size of the macroscopic cluster. To examine of the fluctuations of the system in an ordered state, we created cluster-size histograms for the system. Two particles are defined to be "clustered" together if they are in adjacent (not diagonal) cells. Chains of clustered particles containing s total particles are counted as one cluster of size s. For example, in Figure 3.9, we count one cluster of size four, one of size two, and two of size one.

We measured the time averaged probability that we would find a cluster of size s in the steady-state configuration of the system. This is known as the frequency distribution and denoted $F(s)$. From this, we calculated the residence distribution $R(s) = sF(s)/L$, i.e. the probability to find a randomly selected particle in a cluster of size s. Plots of residency distribution vs. cluster-size for a few values of b and $L = 1000$ are shown in Figure 3.10.

Note that we see a peak at $s = 1$, which corresponds to single particles in the traveler

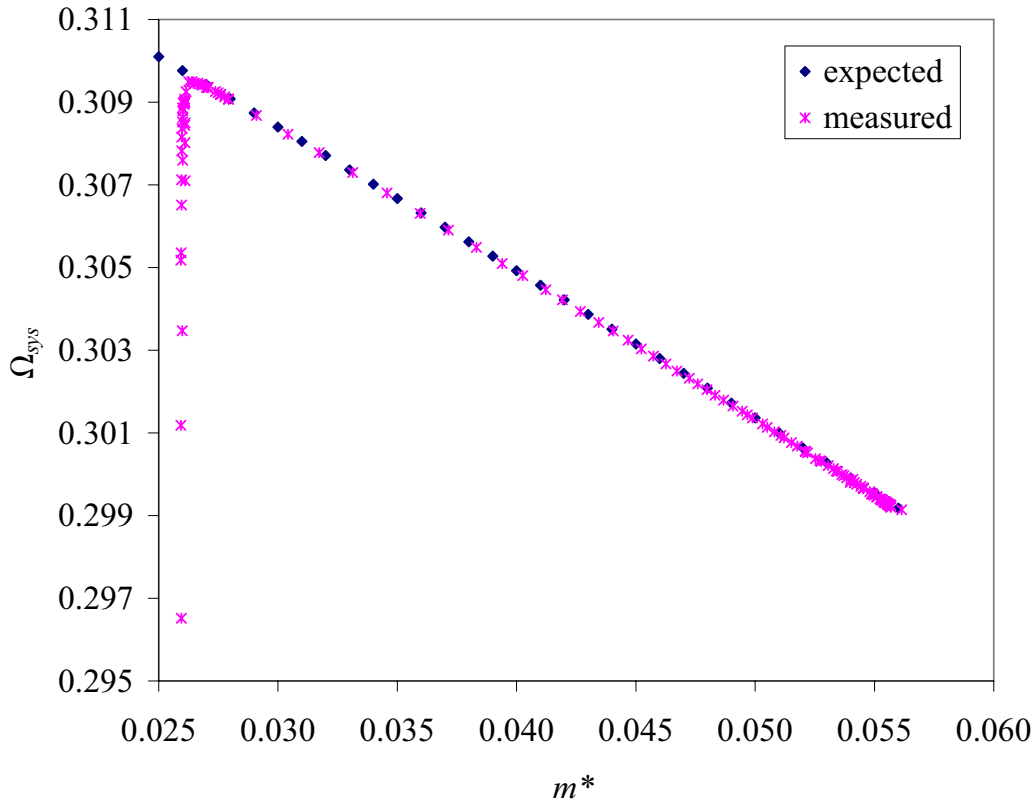

Figure 3.8: Ω_{sys} vs. m^*, for ordered configurations, measured and expected

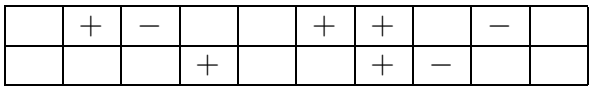

Figure 3.9: Cluster size measurement example: one cluster of size four, one of size two, and two of size one

region, and a larger peak corresponding to the macroscopic cluster at $s \approx 950$. The latter peak occurs for an s that is the most probable size of the macroscopic cluster in the ordered state. These peaks are enlarged in the inset. It comes as no surprise, then, that this value increases with b, consistent with out finding in Section 3.3 that the system becomes *more ordered* as lane preference increases.

Lastly, having completed a thorough examination of the structure of the steady-state, we examine the movement of particles within that structure through measurement of currents.

3.7 Currents

Non-zero currents are a key feature which distinguish non-equilibrium steady-states from equilibrium steady-states. They also contain significant amounts of information about typical particle trajectories in the system. It is therefore only natural that we measure charge and mass currents in the steady state. Of course, positive and negative particles will travel along the lanes in opposite directions, leading to associated currents. This feature is familiar from systems without lane preference. In addition, however, we now also observe net currents flowing between the lanes. Therefore, our data are carefully separated into "in-lane" and "cross-lane" currents.

3.7.1 In-Lane Currents

Let us begin here by defining the local in-lane current of positive particles, $I_{il}^{+}(x,y)$. This is defined as the number of positive particles moving from site (x,y) to site $(x+1,y)$ *minus* the number moving from site (x,y) to $(x-1,y)$, per Monte Carlo step, averaged over the run. Note, then, that because the latter move is not allowed, $I_{il}^{+}(x,y) \geq 0$. The local in-lane current of negative particles, $I_{il}^{-}(x,y)$, is defined in an analogous way where $I_{il}^{-}(x,y) \leq 0$. We now define mass mobility and charge mobility, the net movement of mass and charge in a lane, respectively, per MCS:

$$M_y^m = \sum_x \left[I_{il}^{+}(x,y) + I_{il}^{-}(x,y) \right] \tag{3.3a}$$

$$M_y^q = \sum_x \left[I_{il}^{+}(x,y) - I_{il}^{-}(x,y) \right] \tag{3.3b}$$

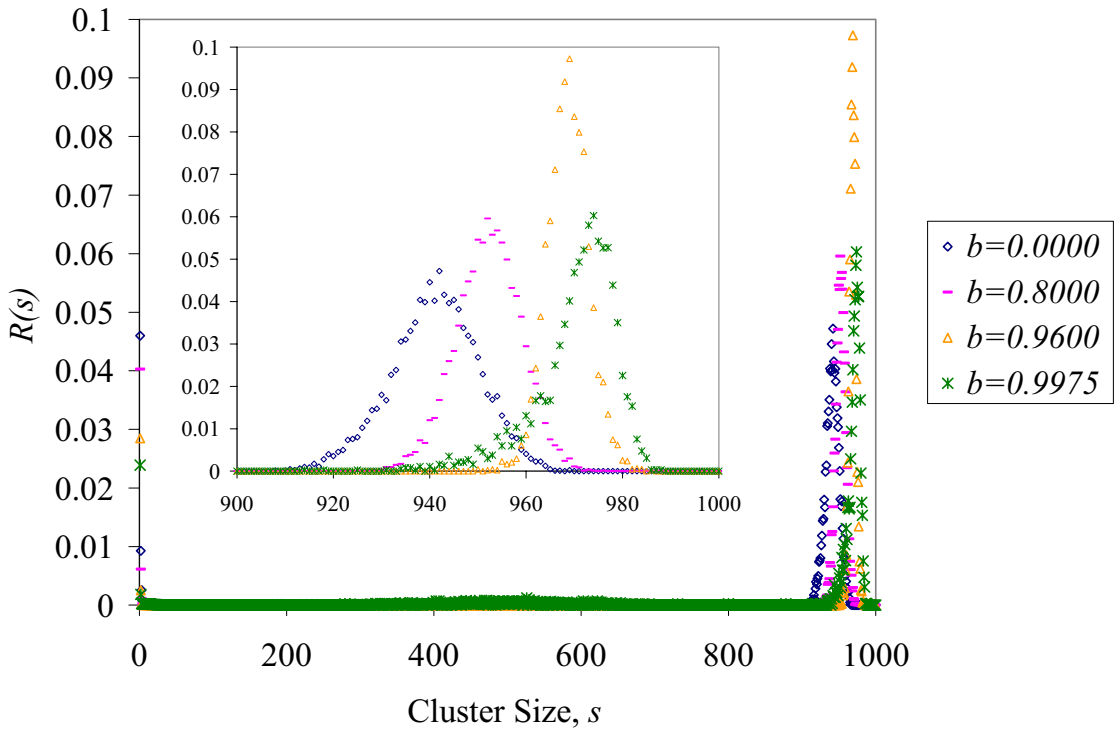

Figure 3.10: Steady-state $R(s)$ vs. s, b for $L = 1000$; Inset: Peaks of residency distribution

The mobilities have somewhat counterintuitive meanings, so we will discuss each before delving into the data. Because mass mobility is the net flow of particles through a lane, $M_y^m = 0$ does not imply "no movement." Note, in particular, that there is no net movement of mass for any particle-particle exchange (PPE). In other words, a vanishing mass mobility only tells us that in a lane, the number of positive particles moving right balances (on average) the number of negative particles moving left. On the other hand, charge mobility is the net flow of charge through a lane, or the number of +'s moving right plus the number of −'s moving left (averaged over the run). Hence, $M_y^q = 0$ can only occur when the positive and negative particles no longer sense a preferred direction, i.e. performed *unbiased* random walks microscopically.

Symmetry dictates certain features of the stationary-state mobilities. First, the sum of the mass mobilities in the two lanes should be zero. Second, the charge mobilities in each lane should be equal. Thus, we need only look at the mobilities in lane 1. Figure 3.11 shows steady-state values for these observables as they depend on b. Only values for ordered states are shown due to size constraints; for completeness both mobilities in the disordered states are ≈ 83 moves per Monte Carlo step.

Note that charge mobilities are monotonically decreasing with b (until the phase transition). This indicates that fewer particles are moving through the system, which is not particularly surprising in light of the evidence, found in previous sections, that the system becomes more "blocked" as the transverse bias increases. The mass mobilities, however, have a local maximum that is very similar to that in the relationship in Figure 3.7 between the traveler charge density q_1^* and b. This indicates that there is a prominent relationship between q_1^* and M_y^m. This is intuitively reasonable because the traveler region is virtually the only region of the system where particles move by PHE, and the more charge-segregated the lanes of the traveler region, the less restricted the movement of particles will be in that region. This relationship is explored further in Section 4.2.3.

3.7.2 Cross-Lane Currents

To measure the currents across the lanes, we count the number of each of the four possible moves - positive or negative particles moving from lane 0 to 1 or 1 to 0 - at each x, per Monte Carlo step, averaged over the run. At each measurement step - every 100 MCS or so - the profile is standardized by shifting it, as discussed in Section 2, so that the center of mass occurs at $x_0 = L/2$. To emphasize the symmetries of the system, we defined "favored" moves as those that occur with rate 1 (+: lane $0 \to 1$, −: lane $1 \to 0$) and "unfavored" moves as those that are suppressed by the transverse bias and occur with rate $1-b$ (+: lane $1 \to 0$, −: lane $0 \to 1$). The former are denoted by an "f" (I_f^+, I_f^-) and the latter by a "u" (I_u^+, I_u^-). Note that in contrast to our mobility measurements from the previous section, we retain spatial dependence in our cross-lane currents.

As mentioned in Section 3.4, profiles develop regions in which only a single species is

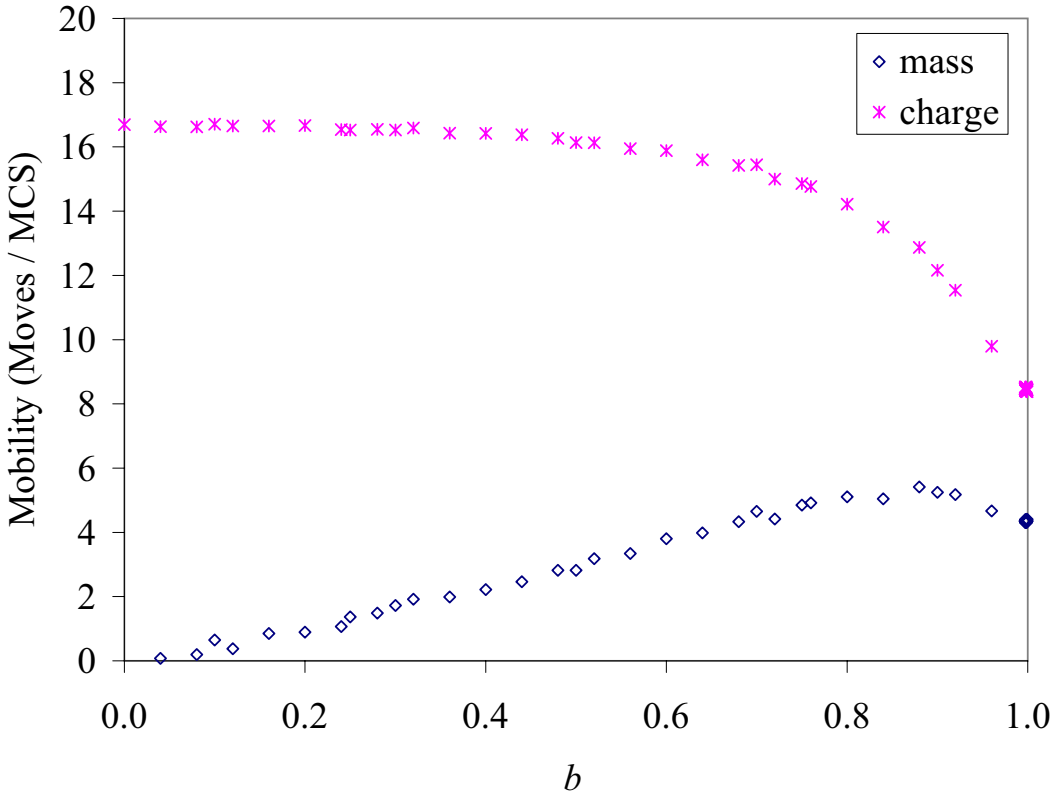

Figure 3.11: Steady-state M_1^m and M_1^q vs. b for $L = 1000$, ordered states only

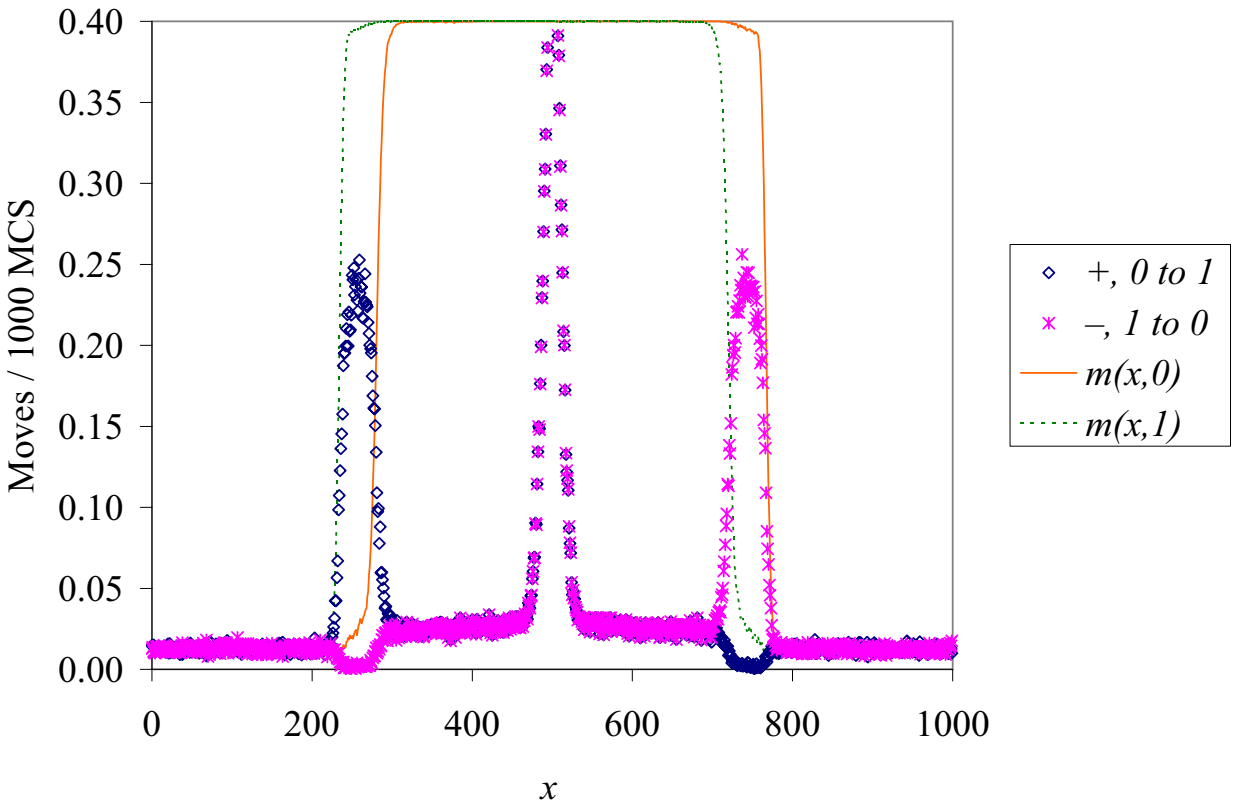

Figure 3.12: Profile of favored cross-lane moves in near-transition system; Mass densities shown for spatial comparison

present as the transition is approached. This simplicity creates a wide array of phenomena, an example of which is an intriguing cross-lane current profile. Figure 3.12 shows example profiles for the favored particle moves and Figure 3.13 shows profiles for the unfavored moves. Both profiles are for $L = 1000$ and $b = 0.9975$.

Note the different vertical scales in each plot. The symmetry of each plot about $x = L/2$ occurs as a result of Symmetry 1. However, some of the peaks are remarkably distinct - there are places where particles obviously prefer to move across lanes with or against the bias. A background plot of the mass profile, which has been scaled vertically to fit in each plot, helps show where each of these peaks occur relative to the profiles obtained in Section 3.4. Notably, positive (negative) particles move with the bias most often at $x \approx 250$ (750) or $x \approx 500$. These positions correspond, respectively, to the confluence of the mixed and traveler regions of the system and the middle of the system, where the mixed and favored regions of each lane meet. Positive (negative) particles move against their lane preference most often at $x \approx 750$ (250), where the favored and traveler regions of the lanes merge.

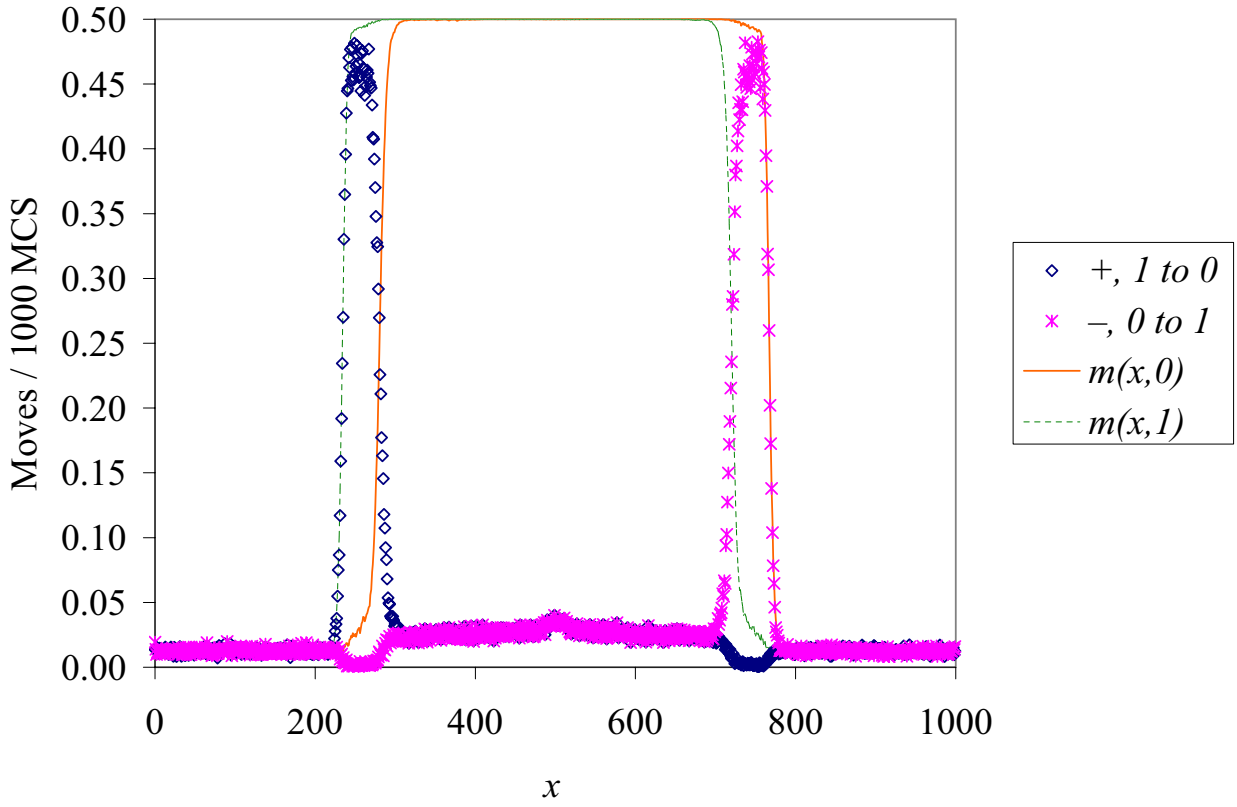

Figure 3.13: Profile of unfavored cross-lane moves in near-transition system; Mass densities shown for spatial comparison

These observations yield a great deal of insight into the dynamics of the system, which will be discussed in Section 4.2.1.

4 Mean-Field Theory

Here we embark on an analytic study of this system from various angles, attempting to probe its behavior in terms of familiar and meaningful quantities. The primary method of analysis is through the mean-field equations of motion. Starting from the master equation, we can derive the evolution equations of the local densities of positive and negative particles, respectively ($\delta_{i,j}$ is the Kronecker delta):

$$p_y(x) \equiv \left\langle \delta_{q(x,y),1} \right\rangle \tag{4.1a}$$

$$n_y(x) \equiv \left\langle \delta_{q(x,y),-1} \right\rangle \tag{4.1b}$$

$$h_y(x) \equiv 1 - p_y(x) - n_y(x) \tag{4.1c}$$

Due to the excluded volume constraint, these equations involve not only averages of local densities, but also their correlations. Away from the transition, a first approximation consists of replacing correlations by products of simple averages or, in other words, assuming that particle probabilities are independent of one another. While this is clearly incorrect - a positive particle is more likely to be to the left of a negative particle than to the right - this mean-field assumption can yield strong insights into the Monte Carlo results. As a result, we obtain four coupled nonlinear equations of motion for the densities of positive and negative particles in each lane:

$$\begin{aligned} \partial_t p_0(x,t) &= (h_0(x,t) + \gamma n_0(x,t))(p_0(x-1,t) + (1-b)\, p_1(x,t)) \\ &\quad - p_0(x,t)(h_0(x+1,t) + \gamma n_0(x+1,t) + h_1(x,t) + \gamma n_1(x,t)) \end{aligned} \tag{4.2a}$$

$$\begin{aligned} \partial_t n_0(x,t) &= (h_0(x,t) + \gamma p_0(x,t))(n_0(x+1,t) + n_1(x,t)) \\ &\quad - n_0(x,t)(h_0(x-1,t) + \gamma p_0(x-1,t) + (1-b)\,(h_1(x,t) + \gamma p_1(x,t))) \end{aligned} \tag{4.2b}$$

$$\begin{aligned} \partial_t p_1(x,t) &= (h_1(x,t) + \gamma n_1(x,t))(p_1(x-1,t) + p_0(x,t)) \\ &\quad - p_1(x,t)(h_1(x+1,t) + \gamma n_1(x+1,t) + (1-b)\,(h_0(x,t) + \gamma n_0(x,t))) \end{aligned} \tag{4.2c}$$

$$\begin{aligned} \partial_t n_1(x,t) &= (h_1(x,t) + \gamma p_1(x,t))(n_1(x+1,t) + (1-b)\, n_0(x,t)) \\ &\quad - n_1(x,t)(h_1(x-1,t) + \gamma p_1(x-1,t) + h_0(x,t) + \gamma p_0(x,t)) \end{aligned} \tag{4.2d}$$

The different terms in these equations can be interpreted as gain or loss terms for the occupancy of site x. A detailed derivation of this equation is provided in Appendix B.

We first integrate these equations numerically to see which features of the Monte Carlo simulations are reproduced by this simple approximation.

4.1 Numerical Integration

When performing the numerical integration, we mimic the Monte Carlo simulations as much as possible, using similar length runs, system sizes, and initial conditions. Discretizing time,

we obtain the following evolution equations:

$$p_0(x, t+\tau) = p_0(x,t) + \tau \partial_t p_0(x,t) \tag{4.3a}$$

$$n_0(x, t+\tau) = n_0(x,t) + \tau \partial_t n_0(x,t) \tag{4.3b}$$

$$p_1(x, t+\tau) = p_1(x,t) + \tau \partial_t p_1(x,t) \tag{4.3c}$$

$$n_1(x, t+\tau) = n_1(x,t) + \tau \partial_t n_1(x,t) \tag{4.3d}$$

The derivatives on the right hand sides, e.g. $\partial_t p_0(x,t)$, are calculated via the mean-field equations (4.2). We use a time step of $\tau = 0.1$. Calculations of observables are performed as in the Monte Carlo case, with $m(x,y) = p_y(x) + n_y(x)$ and $q(x,y) = p_y(x) - n_y(x)$.

Figure 4.1 shows MF steady-state order parameter for varying b and is analogous to the Figure 3.2, which shows the same data for Monte Carlo simulations. The two graphs are nearly identical; we see ordered states for $0 \leq b \lesssim 0.999$, and disordered states for the remainder of b's. However, note that for $0.95 \lesssim b \lesssim 0.999$, the MF plot gives two Ω_{sys} values for each b. This is because numerical integration of the mean-field equations in this region can yield *either* an ordered or disordered steady-state, depending on the initial conditions of the run. Completely ordered initial conditions converge to an ordered state, while a run starting from disorder approaches a disordered state. However, because only one of the steady-states is found in Monte Carlo simulations, this finding more likely indicates a metastability in the MF equations rather than the existence of two "true" steady-states. To understand what is meant by "metastability," consider a system at near the transition (but in the ordered regime) starting from a disordered initial configuration. As we imagine this system at b increasing toward the transition, particles will interfere less with each other's movement, and small blockages that form will disperse more quickly. Therefore, it will require a larger fluctuation to block the lanes sufficiently to create a macroscopic cluster. As b increases, the system will have to wait longer and longer for such a fluctuation, and therefore can appear to have reached a steady-state. This is metastability. (Of course, the reverse situation can also exist, where an ordered initial configuration requires a large fluctuation to reach the disordered steady-state.) Since one effect of the mean-field approximation is to reduce fluctuations as compared to Monte Carlo simulations, it makes sense that metastability would be observed most readily in the integration of the MF equations.

In Figure 4.2, we see that the mean-field equations reproduce the relationship between Q_1 and b, an important result from the Monte Carlo simulations (Figure 3.5). In particular, we see, as in the MC data, that for $L = 1000$ there is a region where increasing the lane preference results in a decrease in the charge of lane 1.

Figure 4.3 shows charge profiles at varying lane preferences for the mean-field integration steady-states. The figure is analogous to Figure 3.6, which gives charge profiles at the same b's for Monte Carlo simulations. Notice that the prominent features of the MC profiles are retained in the integration of the MF equations.

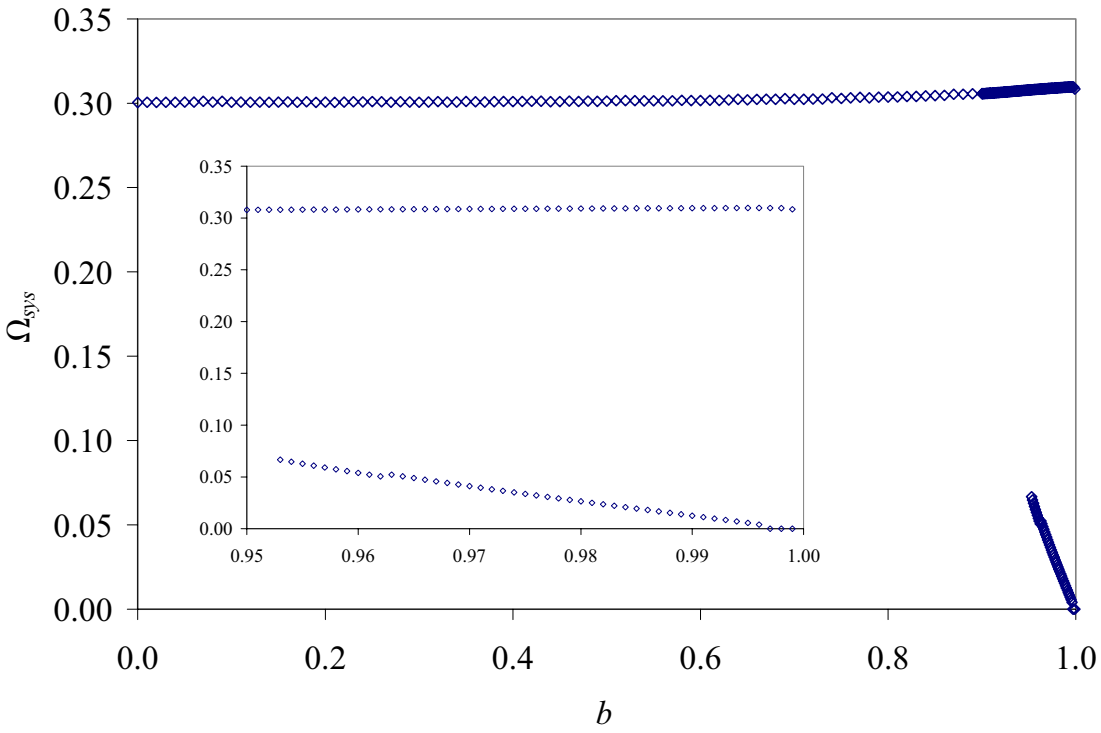

Figure 4.1: MF Ω_{sys} vs. b for $L = 1000$; Inset: Dual steady-states in high-b regime

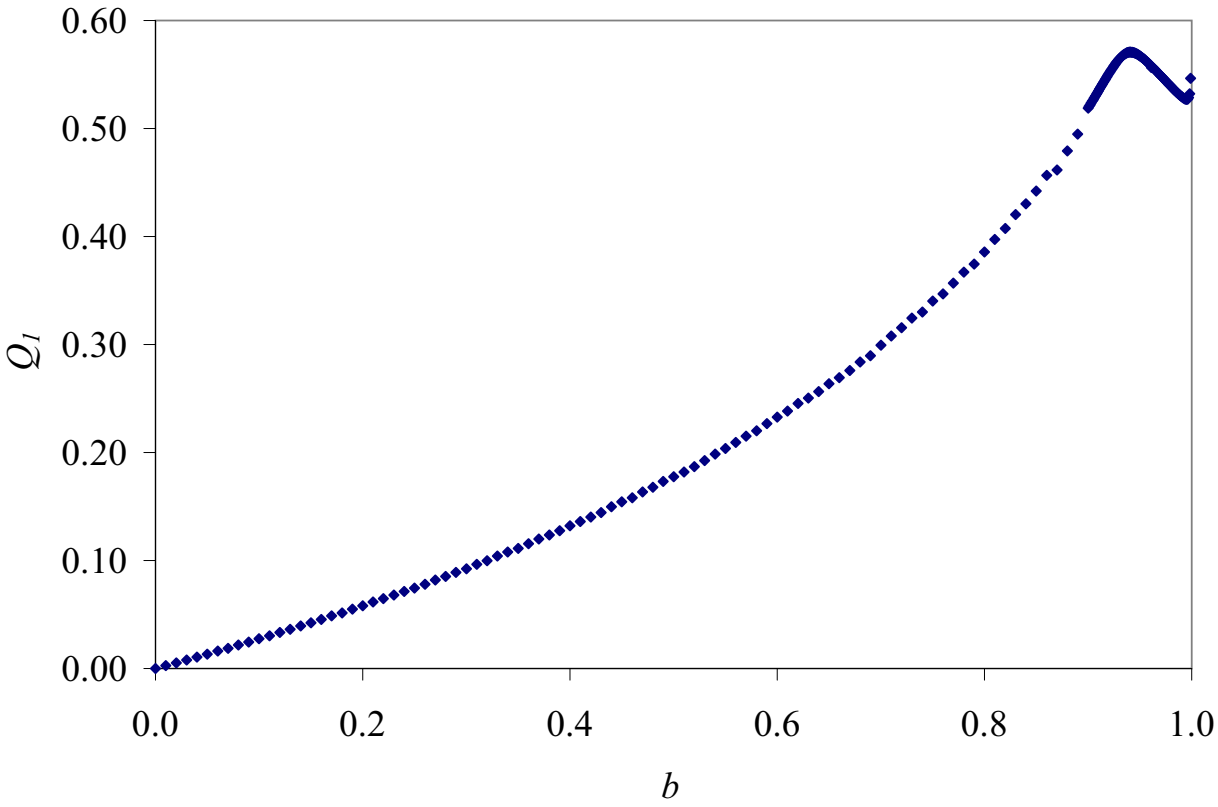

Figure 4.2: MF Q_1 vs. b for $L = 1000$

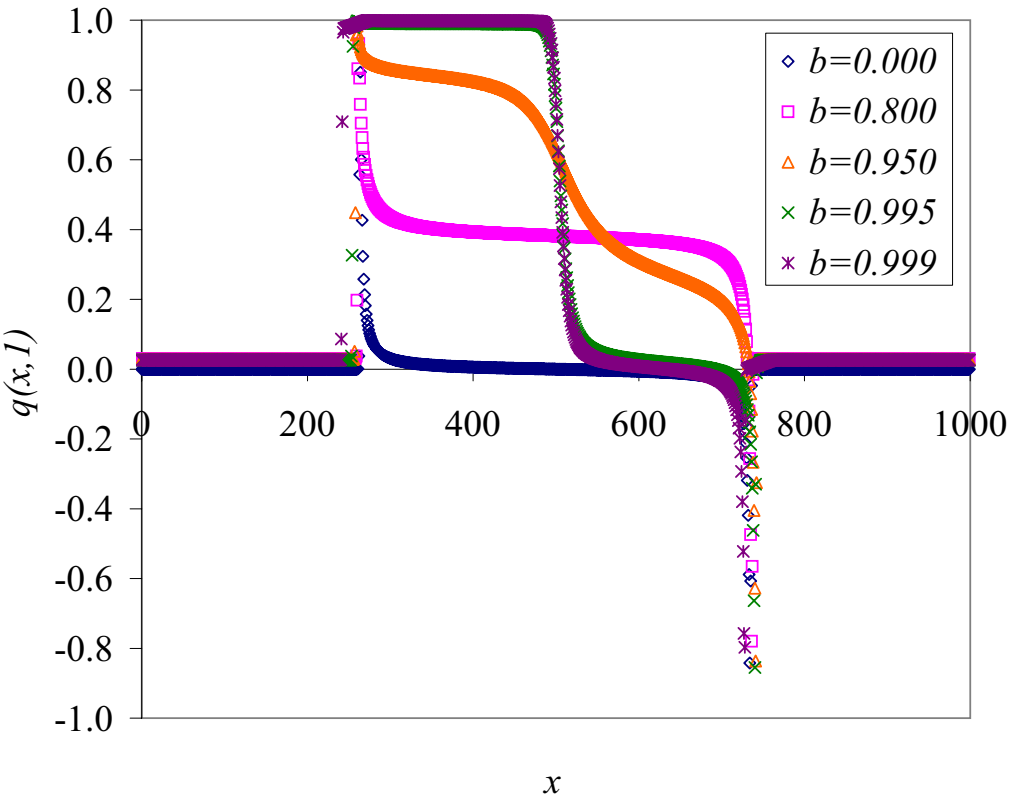

Figure 4.3: MF charge profiles ($\langle q(x,1)\rangle$ vs. x) for various b's, $L = 1000$

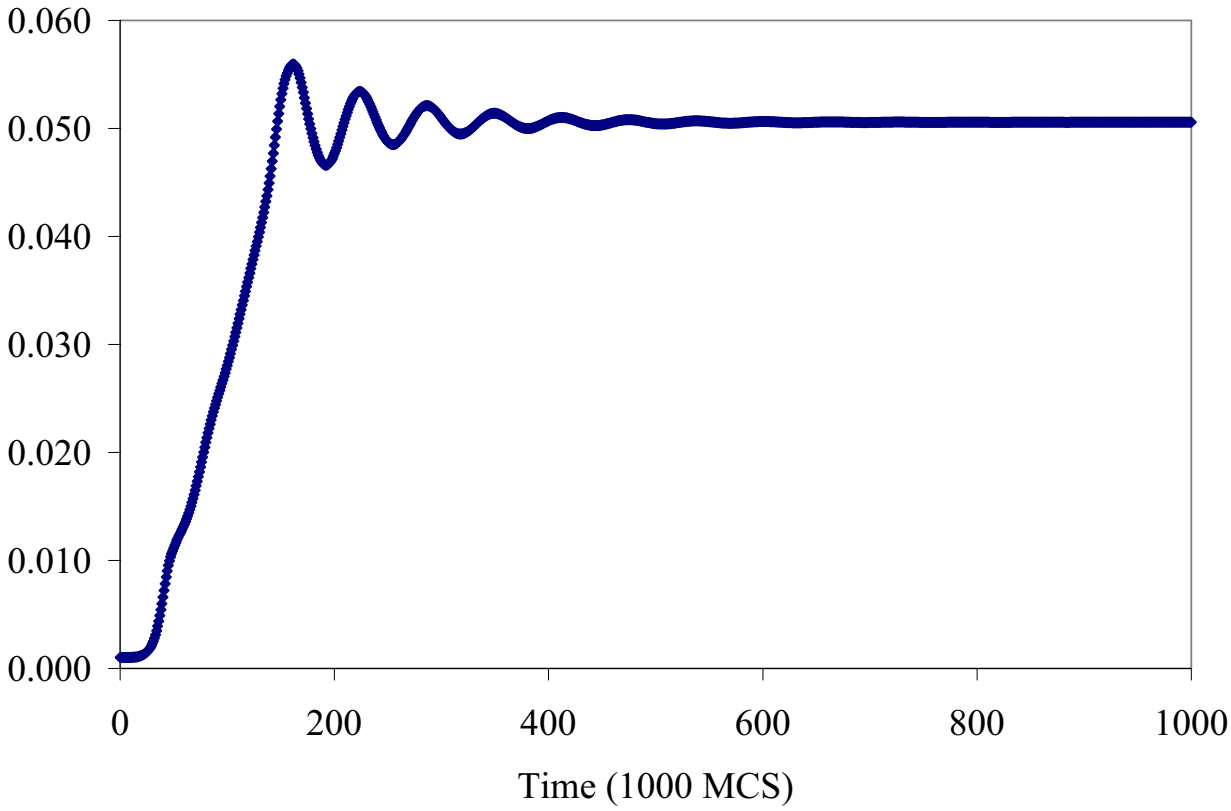

Figure 4.4: Typical time-trace of $\tilde{m}_{sys}$ approaching a disordered state, numerical integration of MF equations

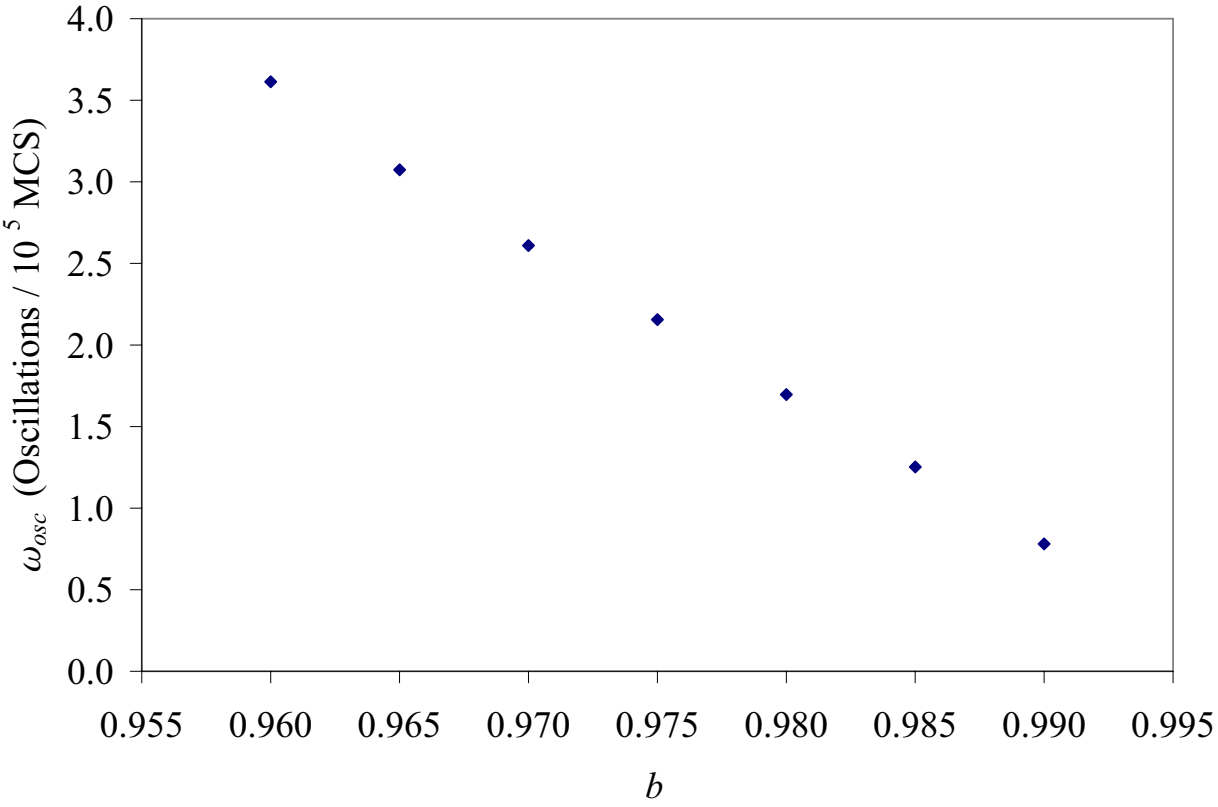

Figure 4.5: $\tilde{m}_{sys}$ oscillations per 10^5 MCS vs. b for $L = 1000$

Lastly, we present Figure 4.4 strictly as a curiosity. It shows a time-trace of $\tilde{m}_{sys}$ for a system reaching a disordered steady-state. Notice the oscillatory behavior of the $\tilde{m}_{sys}$, a characteristic typical of the evolution of disordered states in the MF integration. This indicates an inherent characteristic frequency ω_{osc} of $\tilde{m}_{sys}$ in the mean-field equations. Estimations of this value from the MF results indicates that this frequency is dependent on transverse bias through what appears to be a linear relationship between ω_{osc} and b, as shown in Figure 4.5. The linear fit gives $\omega_{osc} = 0$ for a perfect bias across the lanes ($b = 1$).

This section has shown via numerical integration that the mean-field equations are sufficient for describing the behavior of the system. We now present an analytic examination of the system using these equations, conservation laws, and symmetries.

4.2 Analytical Results

4.2.1 Cluster Near Transition

We begin this discussion by recalling that near the transition, the system develops a simplified three-region structure (see Section 3.4). We will exploit this by analyzing the movement of positive particles in this system, using simple arguments including conservation laws and mean-field theory. Flows of negative particles are analogous and are dictated by Symmetry 1. The result will be a long string of predictions which we test against our Monte Carlo results. Keep in mind, however, that we rely heavily on this structure and most of the arguments fail for b away from the transition.

Near the transition, the system has three distinct regions: (1) the traveler region consisting of a low densities of freely moving particles, (2) a "favored" region consisting almost entirely of the species preferring that lane, and (3) an approximately charge-neutral or "mixed" region. The three regions are evident in the charge profiles for $b = 0.995$ and 0.9989 in Figure 3.6. Also, recall that the clusters in the two lanes become offset near the transition, i.e., there is a portion of the favored region in each lane that lies across from the traveler region in the opposite lane. Figure 4.6 gives a simplistic but instructive diagram of the structure of the system near criticality.

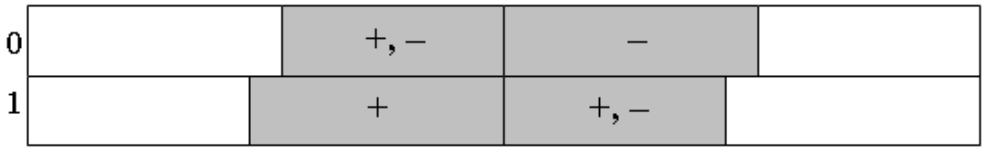

Figure 4.6: Diagram of three-region state of system near the transition; white denotes the traveler region, gray the cluster; favored regions are marked by the species they contain, mixed regions by both species

First of all, note that near the transition, the bias across the lanes is exceedingly strong, so that the traveler region can be considered charge-segregated: positive travelers are only found in lane 1. (In Section 4.2.3, we will calculate $n_1 = m^* \frac{1-b}{2-b}$, or ≈ 0 for purposes here.) So we have a flow of positive particles in lane 1 of the traveler region, and none in lane 0. Second, because the favored regions are entirely composed of one species of particles, they can carry neither charge nor mass current; instead, they act as blockages around which all (net) currents must flow. Third, positive particles flow through each of the mixed regions via PPE. By particle conservation, then, we expect to have two regions with large cross-lane positive particle flows: (1) the center of the cluster, where +'s go from lane 0 to lane 1 and (2) the left (low-x) end of the cluster, where +'s go from lane 1 to 0. Elsewhere, cross-lane currents are minimized due to either the large value of b (the traveler region) or the

presence of +'s in the opposite lane (the remainder of the mixed region). In support of these statements, we recall Figures 3.12 and 3.13 from Section 3.7.2 which showed peaks in the movement of positive particles across lanes in exactly these regions. So we have a complete current loop, diagrammed in Figure 4.7. Keep in mind that these are the only (net) flows of positive particles in the system and, by particle conservation, all must be equal.

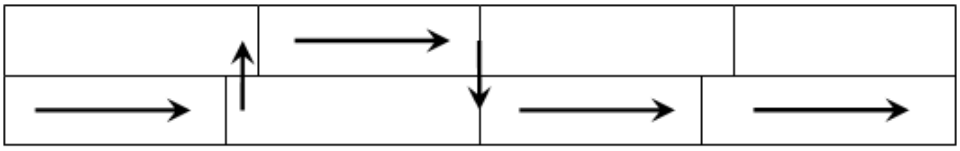

Figure 4.7: Flow of positive particles for high b

We will now calculate these currents and use their equality to generate some useful results. The in-lane current of positive particles, i.e., the rate at which a positive particle moves right, is given by $\left\langle \delta_{q(x-1,y),1}\delta_{q(x,y),0} + \gamma\delta_{q(x-1,y),1}\delta_{q(x,y),-1} \right\rangle$. Applying the mean-field approximation and equation (4.1), we get

$$I_{il}^{+}(x,y) = \frac{1}{3}\left[p_y(x-1)h_y(x) + \gamma p_y(x-1)n_y(x)\right] \tag{4.4}$$

The factor of 1/3 is included to normalize the current to units of "moves per MCS" because each direction (right, left, or across lanes) is chosen once every 3 MCS. Applying this equation to the traveler region of lane 1 where $p_1(x) = m^*$ and $n_1(x) = 0$ yields the positive particle current of the region (which is independent of x by particle conservation):

$$I_{il,trav}^{+}(1) = \frac{1}{3}p_1(x-1)h_1(x) = \frac{1}{3}m^*(1-m^*) \tag{4.5}$$

Now we focus on the mixed region, which is devoid of holes. Note that at the left end of the region, there are more positive particles than negative ones. Similarly, at the right end, there are more negative than positive particles. This can be observed by looking at the charge profile of the mixed region in Figure 3.6, or simply stated by reasoning that positive (negative) particles are more likely to be on the left (right) side of any cluster. It follows then that there must be an x in between such that the numbers of each are equal, i.e., $n_1(x) = p_1(x) = \frac{1}{2}$. Then the positive particle current at that x - and, by particle conservation, throughout the mixed region - is

$$I_{il,mix}^{+}(1) = \frac{1}{3}\gamma p_1(x-1)n_1(x) = \frac{\gamma}{12} \tag{4.6}$$

Setting this current equal to $I_{il,trav}^{+}(1)$, we get an equation for the traveler density:

$$m^* = \frac{1}{2} - \frac{1}{2}\sqrt{1-\gamma} \tag{4.7}$$

Note that this value is independent of b (except that it be low enough that the three-region structure can form) and system size. For $\gamma = 0.1$ this yields $m^* = 0.02566$ in good agreement with the high-b value measured in Section 3.5.

Note that the positive particles in the mixed region of lane 0, especially those towards its left edge, stabilize the cluster - in their absence, negative particles would immediately escape and the cluster would disintegrate very quickly. We refer to these particles (and their negative counterparts in lane 1) as the "gatekeepers." They are generated when positive particles move into lane 0. We will look at this "gatekeeper generation" current next.

At the ends of the cluster, the two lanes are offset a small amount; there are a few sites of the favored region in lane 1 that overlap with the traveler region of lane 0. We denote the width of this region by Δ. Gatekeepers are generated when positive particles in this overhang make the *suppressed* move to lane 0 and are *prevented* from jumping back. This leads to a current - the "gatekeeper generation current" - which we will now attempt to compute. To understand the sequence of events involved, we first note that a such a suppressed move generates a particle-hole pair, with the positive particle now in lane 0 and the hole in lane 1. If this pair is selected for another exchange attempt in the course of the simulation, the positive particle will return to lane 1. In this case, no gatekeeper has been generated. In other words, the positive particle can stay in lane 0 only if it is separated from its hole partner. This can occur in two ways: either (a) the particle moves right in lane 0 (by exchanging with a hole or one of the 'traveling' negative particles there), or (b) the hole moves left, by exchanging with a positive particle in lane 1. We emphasize that this is the only region in the system where such a sequence of events is likely to occur and lead to a particle trapped in the wrong lane.

Before we calculate the gatekeeper generation current, I_g, notice that this is not a single cross-lane current, but a composition of all cross-lane currents for $x \in$*offset*. Figure 4.8 illustrates these small currents that sum to I_g, and can be thought of as an enlarged view of the offset region in Figure 4.7.

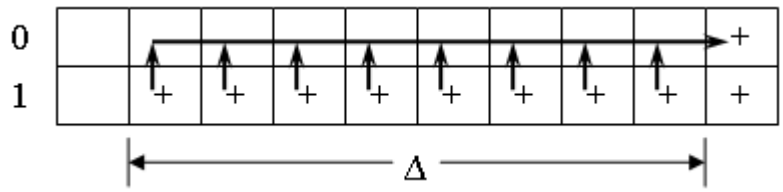

Figure 4.8: Cross-lane currents composing I_g

Now, we are ready to write down the gatekeeper generation current in terms of Δ and the

probability α that the lane 0/lane 1 particle/hole pair is separated before it can exchange a second time.

$$I_g = \sum_{x \in \text{offset}} \left[I_u^+(x) - I_f^+(x) \right] = \frac{1}{3}(1-b)p_1 h_0 \alpha \Delta = \frac{1}{3}\alpha\Delta(1-b)(1-m^*) \tag{4.8}$$

Since this current is also part of the loop in Figure 4.7, it is equal to the other currents. Then, setting $I_g = I^+_{il,mix}(1)$, we get an equation for Δ:

$$\Delta = \frac{\gamma}{4\alpha(1-b)(1-m^*)} = \frac{\gamma}{2\alpha(1-b)(1+\sqrt{1-\gamma})} \tag{4.9}$$

Note the surprising result that Δ does not scale at all with system size; it is entirely independent of L. Mean-field calculations based on the dynamics of the system yield $\alpha \approx \frac{2}{3}$ (see Appendix C for details) and thus we predict $\Delta = 35.0$ for $b = 0.9989$. Using our Monte Carlo data to extract Δ for different values of b and L, we confirm that Δ does indeed appear to be independent of L; however, it differs quanitatively from our prediction, e.g. $\Delta = 46.5$ for $b = 0.9989$ in the simulations.

To understand the discrepancy, we attempted to extract an empirical value for α from the data shown in Figures 3.12 and 3.13. In particular, we will look at the peaks of unfavored and favored cross lane currents in the offset region of lane 1 ($x \approx 250$). It is natural to identify the area under the unfavored peak (denoted U), which measures the number of positive particles moving into lane 0, with the number of gatekeepers created. Similarly, we identify the area under the favored peak (F), which measures the number of positive particles moving into lane 1, with the number of gatekeepers immediately destroyed after creation. Then we can measure α: $\alpha = 1 - \frac{F}{U} \approx 0.5$, much different from our analytic estimate. Using this value of α and returning to our equation, we get $\Delta = 46.6$, quite close to the measured value. This, along with the L independence, indicates that equation (4.9) is correct, but our theoretical estimate of α is not. Clearly, further studies are required to fully understand the origin of α.

Note that these gatekeepers - positive particles in the mixed region of lane 0 - move along the lane via PPE until they reach the end of the mixed region. Then they make the *unsuppressed* jump back to lane 1 by exchanging with a negative particle in lane 0 - a gatekeeper from the opposite end of the cluster - resulting in the favored cross-lane current peak that we see in the middle of the system in Figure 3.12. This indicates that the mixed regions of opposite lanes share an endpoint, and also that Δ is the difference between the lengths of the favored and mixed regions. The lengths of the regions can then be calculated:

$$L_m = \frac{L}{2}(1 - Q_1) \tag{4.10a}$$

$$L_t = \frac{L}{2(1-m^*)} \tag{4.10b}$$

$$L_f = Q_1 - m^* L_t = \frac{L}{2} Q_1 - \frac{L m^*}{2(1-m^*)} \tag{4.10c}$$

The first and second equations derive from the fact that the mixed and traveler regions contain all of the negative particles and holes, respectively, in lane 1. The favored region contains all of the net charge not in the traveler region, resulting in the third relation. Setting $\Delta = L_f - L_m$ and rearranging, we arrive at an equation for Q_1:

$$Q_1 = \frac{\Delta}{L} + \frac{1}{2(1-m^*)} \tag{4.11}$$

Using the measured α, this yields a prediction of $Q_1 = 0.560$ for $b = 0.9989$, within 1.5 percent error of the measured value 0.567.

The lane and system order parameters can also be calculated from equations (4.10):

$$\Omega_{sys} = \frac{(1-m^*)\, sin\left(\frac{\pi}{2(1-m^*)}\right) cos\left(\frac{\pi\Delta}{L}\right)}{L sin\left(\frac{\pi}{L}\right)} \tag{4.12a}$$

$$\Omega_y = \frac{(1-m^*) sin\left(\frac{\pi}{2(1-m^*)}\right)}{L sin\left(\frac{\pi}{L}\right)} \tag{4.12b}$$

Detailed derivations of these equations are performed in Appendix A. Note that the lane calculation is identical to that for an ordered system with no offset, and thus yields the same result as equation (3.2). The resulting values of $\Omega_y = 0.30988$ and $\Omega_{sys} = 0.30656$ compare well with measured values of $\Omega_y = 0.30937$ and $\Omega_{sys} = 0.30612$.

Table 4.1 summarizes the analytical results from this section as compared with values measured from Monte Carlo simulations for $L = 1000$ and $L = 10000$.

	$L = 1000$			$L = 10000$		
Observable	Measured	Predicted	Error	Measured	Predicted	Error
m^*	0.02595	0.02566	1.12%	0.02566	0.02566	0.018%
α	0.501	0.6641	32.6%	0.5068	0.6641	31.0%
Δ	46.5	46.6†	0.126%	46	46.02†	0.052%
Q_1	0.560	0.567†	1.28%	0.5137	0.5177†	0.768%
Ω_{sys}	0.30612	0.30612†	0.147%	0.30984	0.30985†	0.002%
Ω_y	0.30937	0.30988†	0.164%	0.30987	0.30988†	0.004%

Table 4.1: Summary of results, analysis of the system near transition. Both system sizes are for $b = 0.9989$. † indicates that the measured value of α was used in the prediction.

Lastly, it is worth acknowledging that we did not utilize the fourth flow of positive particles, namely the favored cross-lane current in the middle of the cluster. We were unsuccessful in performing calculations with it that yielded any useful results.

4.2.2 Charge in Favored Region

As noted above, lane 1 contains a region which is almost completely filled with positive particles. The charge profile is nearly 1 in this region (see Figure 3.6); here, we compute its average value. Let us assume for simplicity that the favored region has uniform particle densities p_1 and n_1; this seems reasonable given the profiles in the figure. Then our steady-state mean-field equation for motion across the lanes is

$$(1-b)\gamma p_1 n_0(x) - \gamma n_1 p_0(x) = 0 \tag{4.13}$$

Integrating across the region yields the ratio $(1-b)\frac{p_1}{n_1} = \frac{\int p_0(x)}{\int n_0(x)}$. If we assume that the mixed region of the opposite lane contains equal numbers of positive and negative particles (again, reasonable given the charge profile), the term on the right is 1. Then this, coupled with the assumption that lane 1 is filled ($p_1 + n_1 = 1$), gives a value for charge in the favored region of lane 1 as a function of b:

$$q_1^f = p_1 - n_1 = \frac{b}{2-b} \tag{4.14}$$

Figure 4.9 tests this formula against measured values. Notice the small horizontal and vertical scales. We see that the measured value is significantly less than calculated for $b \approx 0.95$, but approaches expectations rapidly as $b \to 1$. The inset shows the difference between the two values as a function of b. Again, notice the small scales - the difference becomes extremely small for $b > 0.99$, or approximately where the system attains the three-region structure.

4.2.3 Traveler Charge Density and Mass Mobility

In Section 3.7.1, we pointed out the similarity between plots of traveler charge density vs. b (Figure 3.7) and mass mobility vs. b (Figure 3.11), and hinted at reasons for such a relationship. Here, we will use mean-field theory to calculate a relationship between these two variables via the traveler mass density (m^*). First, recall that non-zero mass mobilities only occur where particles move via particle-hole exchanges (outside the cluster). Thus, the mass current depends on the traveler mass density m^* and the rate with which the particles move in the traveler region.

We assume that the traveler region is so sparsely populated that they interfere only very rarely with one another. Therefore, we may treat the density of each species in each lane as uniform across the traveler region: $p_1(x) = p_1$ and $p_0(x) = p_0$, and by symmetry $n_1 = p_0$

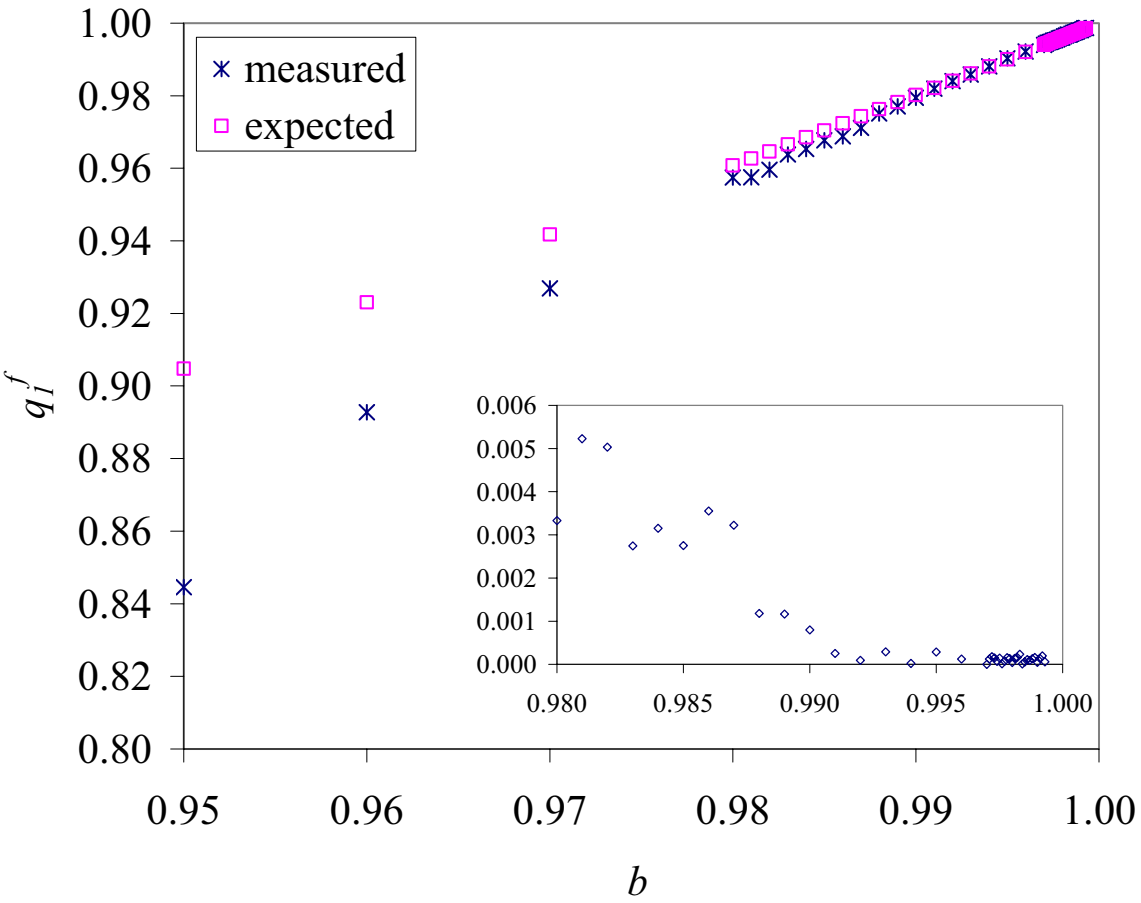

Figure 4.9: Measured and expected values for charge in the favored region of the cluster vs. b; Inset: Difference between measured and expected values

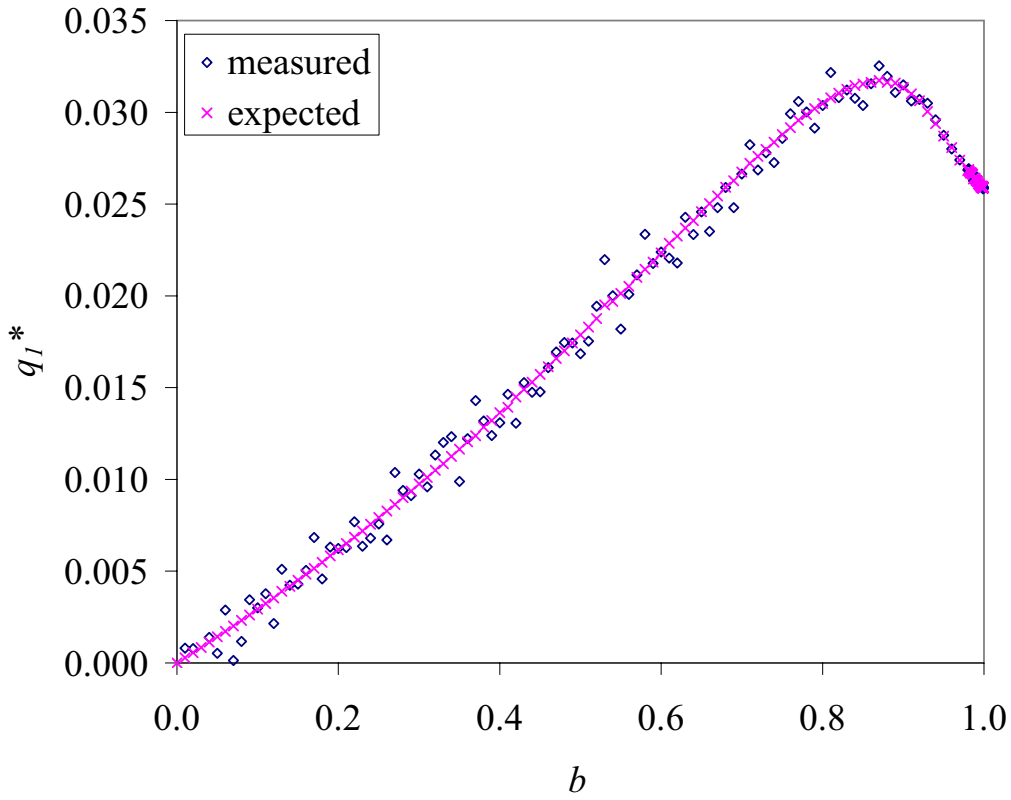

Figure 4.10: Measured and expected values for traveler charge density vs. b

and $n_0 = p_1$. This assumption is justified by the constant mass and charge profiles in the traveler region, seen in Figures 3.1 and 3.6. Further, Figures 3.12 and 3.13 demonstrate that there is no net mass flow from one lane to the other throughout the traveler region:

$$p_0(1 - n_1 - p_1) - (1 - b)p_1(1 - p_0 - n_0) = 0 \tag{4.15}$$

Combining these expressions with the definition of the traveler mass density, we obtain $m^* = p_1 + n_1 = p_1 + p_0 = p_1 + (1 - b)p_1 = (2 - b)p_1$. So the particle mass densities are $p_1 = m^*/(2 - b)$ and $n_1 = m^* \frac{1-b}{2-b}$. Also, the charge density in the traveler region follows as

$$q_1^* = p_1 - n_1 = m^* \frac{b}{2 - b} \tag{4.16}$$

Using values of m^* vs. b from the Monte Carlo data, we calculated expected values of q_1^* using this equation. Figure 4.10 shows this result plotted against MC data for q_1^*. We can see that the two curves agree very well, indicating that our approximations were reasonable.

Using our results for p_1 and n_1, we now calculate the mass mobility M_1^m in lane 1, i.e., the net number of particle moves to the right in lane 1 per MCS. Note that for a particle-particle exchange, there is no net movement of mass. Then the only moves that contribute to M_1^m are particle-hole exchanges, which occur exclusively in the traveler region. Therefore, M_1^m is equal to the number of positive particles in the traveler region multiplied by the chances the right-hand direction is chosen (one in three) and the chances that the move is made (a hole is to the right), minus an analogous term for negative particles. So the equation is:

$$M_1^m = \frac{1}{3}\left(L_t p_1(1-m^*) - L_t n_1(1-m^*)\right) = \frac{L}{6} q_1^* \tag{4.17}$$

The last equality uses equation (4.10b) relating L_t and m^*, which holds for all b since the traveler region always contains (approximately) all of the unoccupied sites. Thus we see that there is a linear relationship between traveler charge density and mass current. Coupling this equation with the previous one relating q_1^* and m^*, we used Monte Carlo data for m^* vs. b to calculate expected values of M_1^m for each b. Figure 4.11 shows excellent agreement between these predicted values and values of M_1^m vs. b measured directly from the MC simulations.

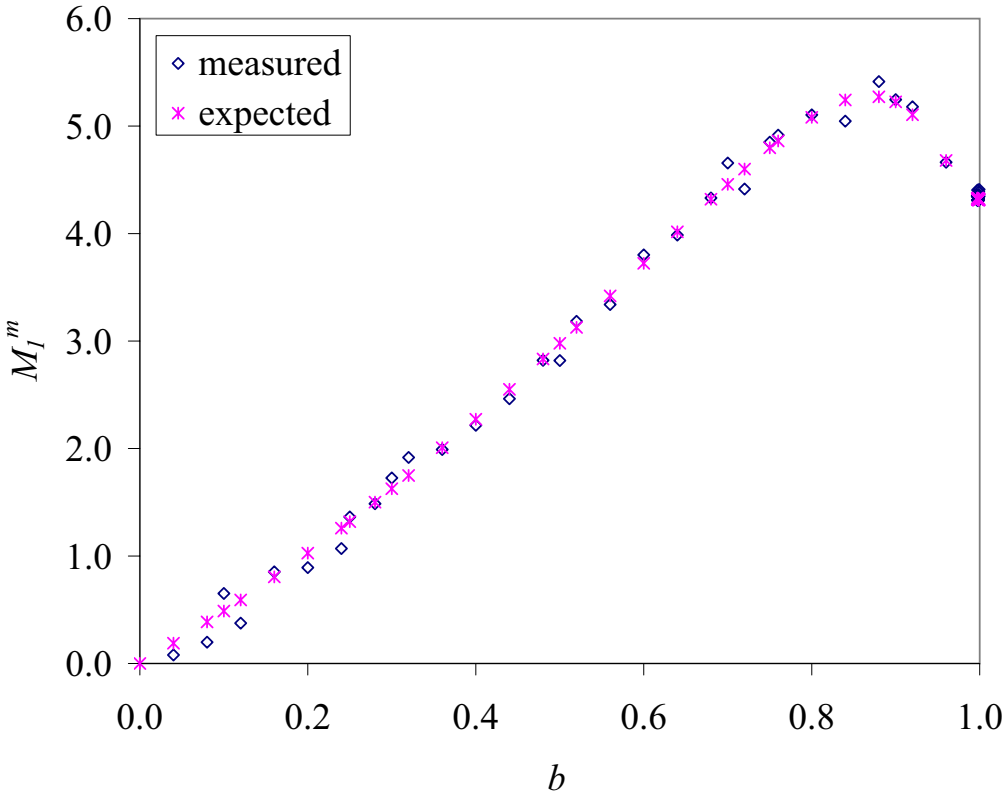

Figure 4.11: Measured and expected values for mass mobility vs. b

5 Conclusion

We analyzed the behavior of two species (+,−) of particles being driven in opposite directions along a $2\times L$ lattice with periodic boundary conditions at half-filling. We generalized previous studies of the symmetric case [5, 6] by imposing a lane preference (denoted b) and observed the resulting deviation in behavior. The model can be interpreted in an intuitive way as fast cars and slow cars preferring the left and right lanes, respectively, and travelling on a 2-lane ring road viewed in a comoving frame of reference. We allow the particles to exchange position with probability $\gamma = 0.1$.

We performed Monte Carlo (MC) simulations of the model for a range of lane preferences, system sizes, and initial conditions. We found that the system remained ordered - the majority of the cars in a single cluster - for all but nearly perfect lane preference. The region outside of the cluster was sparsely populated with "travelers," particles that, having escaped one end of the cluster, move rapidly and relatively uninhibitedly toward the other end.

We measured an order parameter to distinguish between ordered and disordered phases, and saw what appeared to be a first-order (discontinuous) transition between the two. We verified this observation performing a hysteresis loop, decreasing the lane preference from a disordered phase until the transition occurred then increasing back to the disordered phase. We expected to find that increasing the lane preference would decrease the disruption in the traffic, but instead were surprised to see that the cars became more clustered as the bias across the lanes increased. We also measured a range of b's in which increasing the lane preference decreased the charge disparity between the lanes, i.e., made it *less* likely that we would find cars in their preferred lane. In addition, we discovered that the cluster took on an extremely simple form, with long blockages of a single species of particles in each lane, and an offset between the clusters in the lanes that increased near the transition. Current flows across the lanes were recorded and displayed an abnormal profile, the features of which aligned with the structure of the cluster. We tallied the total net movement of charge and mass along each lane in each Monte Carlo step, and recorded histograms of cluster sizes to monitor fluctuations.

We analyzed the model using mean-field (MF) theory and simpled arguments based on symmetry and conservation laws. Numerical integration of the MF equations of motion yielded results similar to those of the MC simulations. We observed an apparent metastability of the mean-field equations near the cluster, resulting in what appeared to be two stable configurations (one ordered, one disordered) near the transition. We were able to reproduce each of the surprising features of the Monte Carlo data mentioned above, indicating that we could utilize the MF equations in our analytic work.

We were able to exploit the species-segregated regions of the cluster near the transition by looking at the currents of positive particles in the system. The result was a long string of successful predictions of observables near the transition, including the density of travelers, the order parameter, lane charge, traveler charge density, and mass mobility. Our results

improved as measurements were taken closer to the transition and system size was increased. We were able to relate traveler density of the system to the charge and mass mobilities, the order parameter, and the cluster size.

After all of this, though, questions still abound and plenty of work remains. An explanation for the massive rearrangment of the cluster at $b \approx 0.95$ needs to be found and might, too, explain why charge decreases during this process. The order parameter increases monotonically with b, and an equation needs to be developed to explain this relationship. The value of the variable α discussed in Section 4.2.1 should be calculable from the dynamics of the system; this would complete the long string of arguments and predictions in that section. A characterization of the entire phase diagram, including variations in γ and the filling fraction, should be completed. A comparison with traffic data might also prove interesting.

References

[1] S. Katz, J.L. Lebowitz and H. Spohn, Phys. Rev. **B28** (1983) 1655; J. Stat. Phys., **34** (1984) 497.

[2] B. Schmittmann and R. K. P. Zia, *Phase Transitions and Critical Phenomena* Vol. 17, eds. C. Domb and J.L. Lebowitz, (Academic Press, N.Y., 1995).

[3] G. Korniss, B. Schmittmann and R.K.P. Zia, Europhys. Lett., **32** (1995) 49; J. Stat. Phys. **86** (1997) 721.

[4] C. Godréche and S. Sandow, private communications

[5] G. Korniss, B. Schmittmann and R.K.P. Zia, Europhys. Lett., **45** (1999) 431.

[6] Y. Kafri, E. Levine, D. Mukamel and J. Török, J. Phys. A., **35** (2002) L459-L466.

[7] D. Chowdhury, L. Sanken, and A. Schadschneider, Phys. Rep. **329**, 199 (2000).

[8] Schmittmann B. and Zia R. K. P., unpublished

Appendix

A Order Parameter Calculations

A.1 Lane or System with Traveler Density m^*

Here we calculate the order parameter for a lane or system (no offset) with mass densities of m^* in the traveler region and 1 in the favored and mixed regions. Then

$$\Omega = \left| \frac{1}{L} \left[\sum_{x=0}^{L_t-1} m^* exp\left(i\frac{2\pi x}{L}\right) + \sum_{x=L_t}^{L-1} exp\left(i\frac{2\pi x}{L}\right) \right] \right|$$

Using the identity $\sum_{x=0}^{n-1} a^x = \frac{a^n - 1}{a-1}$,

$$\begin{aligned}
\Omega &= \left| \frac{1}{L} \left[m^* \frac{exp\left(i\frac{2\pi L_t}{L}\right) - 1}{exp\left(i\frac{2\pi}{L}\right) - 1} + exp\left(i\frac{2\pi L_t}{L}\right) \frac{exp\left(i\frac{2\pi(L-L_t)}{L}\right) - 1}{exp\left(i\frac{2\pi}{L}\right) - 1} \right] \right| \\
&= \frac{1}{L} \left| m^* \frac{exp\left(i\frac{\pi L_t}{L}\right) sin\left(\frac{\pi L_t}{L}\right)}{exp\left(i\frac{\pi}{L}\right) sin\left(\frac{\pi}{L}\right)} + exp\left(i\frac{2\pi L_t}{L}\right) \frac{exp\left(i\frac{\pi(L-L_t)}{L}\right) sin\left(\frac{\pi(L-L_t)}{L}\right)}{exp\left(i\frac{\pi}{L}\right) sin\left(\frac{\pi}{L}\right)} \right| \\
&= \frac{1}{Lsin\left(\frac{\pi}{L}\right)} \left| m^* exp\left(i\frac{\pi L_t}{L}\right) sin\left(\frac{\pi L_t}{L}\right) + exp\left(i\frac{\pi L_t}{L}\right) exp\left(i\pi\right) sin\left(\frac{\pi\left(L-L_t\right)}{L}\right) \right| \\
&= \frac{sin\left(\pi - \frac{\pi L_t}{L}\right) - m^* sin\left(\frac{\pi L_t}{L}\right)}{Lsin\left(\frac{\pi}{L}\right)}
\end{aligned}$$

Since $sin(\pi - x) = sin(x)$,

$$\Omega = \frac{(1-m^*)\, sin\left(\frac{\pi L_t}{L}\right)}{Lsin\left(\frac{\pi}{L}\right)}$$

Lastly, using equation (4.10) for L_t,

$$\Omega = \frac{(1-m^*)\, sin\left(\frac{\pi}{2(1-m^*)}\right)}{Lsin\left(\frac{\pi}{L}\right)}$$

A.2 System with Cluster Offset Δ and Traveler Density m^*

Figure A.1 shows the mass densities of the system. Black (the cluster) and gray (the traveler region) represent $m(x, y) = 1$ and $m(x, y) = m^*$, respectively.

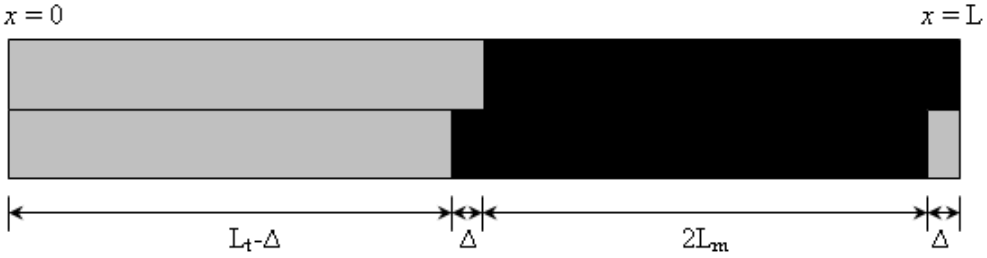

Figure A.1: Mass densities in ordered phase with offset Δ; Black represents $m(x, y) = 1$, gray $m(x, y) = m^*$

We see that there are four regions that have different mass densities (averaged over y): a region of length $L_t - \Delta$ with density m^*, two of length Δ with mass densities $(m^* + 1)/2$, and one of length $2L_m$ with density 1. Then

$$\begin{aligned}\Omega_{sys} &= \left|\frac{1}{L}\left[\sum_{x=0}^{L_t-\Delta-1} m^* exp\left(i\frac{2\pi x}{L}\right) + \sum_{x=L_t-\Delta}^{L_t-1}\left(\frac{m^*+1}{2}\right) exp\left(i\frac{2\pi x}{L}\right)\right.\right. \\ &\quad \left.\left. + \sum_{x=L_t}^{L_t+2L_m-1} exp\left(i\frac{2\pi x}{L}\right) + \sum_{x=L_t+2L_m}^{L-1}\left(\frac{m^*+1}{2}\right) exp\left(i\frac{2\pi x}{L}\right)\right]\right|\end{aligned}$$

Following the same procedure as above and skipping a step or two, we get

$$
\begin{aligned}
\Omega_{sys} &= \frac{1}{Lsin\left(\frac{\pi}{L}\right)}\left|m^{*}exp\left(i\frac{\pi\left(L_t-\Delta\right)}{L}\right)sin\left(\frac{\pi\left(L_t-\Delta\right)}{L}\right)\right. \\
&\quad +\left(\frac{m^{*}+1}{2}\right)exp\left(i\frac{2\pi\left(L_t-\Delta\right)}{L}\right)exp\left(i\frac{\pi\Delta}{L}\right)sin\left(\frac{\pi\Delta}{L}\right) \\
&\quad +exp\left(i\frac{2\pi L_t}{L}\right)exp\left(i\frac{2\pi L_m}{L}\right)sin\left(\frac{2\pi L_m}{L}\right) \\
&\quad \left.+\left(\frac{m^{*}+1}{2}\right)exp\left(i\frac{2\pi\left(L_t+2L_m\right)}{L}\right)exp\left(i\frac{\pi\Delta}{L}\right)sin\left(\frac{\pi\Delta}{L}\right)\right| \\
&= \frac{1}{Lsin\left(\frac{\pi}{L}\right)}\left|m^{*}exp\left(-i\frac{\pi\Delta}{L}\right)sin\left(\frac{\pi\left(L_t-\Delta\right)}{L}\right)\right. \\
&\quad +\left(\frac{m^{*}+1}{2}\right)sin\left(\frac{\pi\Delta}{L}\right)\left(exp\left(i\frac{\pi\left(L_t-\Delta\right)}{L}\right)+exp\left(i\frac{\pi\left(L_t+4L_m+\Delta\right)}{L}\right)\right) \\
&\quad \left.+exp\left(i\frac{\pi\left(L_t+2L_m\right)}{L}\right)sin\left(\frac{2\pi L_m}{L}\right)\right|
\end{aligned}
$$

Using $L_t + 2L_m = L - \Delta$,

$$
\begin{aligned}
\Omega_{sys} &= \frac{1}{Lsin\left(\frac{\pi}{L}\right)}\left|exp\left(-i\frac{\pi\Delta}{L}\right)\left(m^{*}sin\left(\frac{\pi\left(L_t-\Delta\right)}{L}\right)+exp(i\pi)sin\left(\frac{2\pi L_m}{L}\right)\right)\right. \\
&\quad +\left(\frac{m^{*}+1}{2}\right)sin\left(\frac{\pi\Delta}{L}\right)exp\left(i\frac{\pi\left(L_t+2L_m\right)}{L}\right) \\
&\quad \left.\left(exp\left(-i\frac{\pi\left(\Delta+2L_m\right)}{L}\right)+exp\left(i\frac{\pi\left(\Delta+2L_m\right)}{L}\right)\right)\right| \\
&= \frac{1}{Lsin\left(\frac{\pi}{L}\right)}\left|m^{*}sin\left(\frac{\pi\left(L_t-\Delta\right)}{L}\right)-sin\left(\frac{2\pi L_m}{L}\right)\right. \\
&\quad \left.-\left(m^{*}+1\right)sin\left(\frac{\pi\Delta}{L}\right)cos\left(\frac{\pi\left(\Delta+2L_m\right)}{L}\right)\right|
\end{aligned}
$$

Using $\Delta + 2L_m = L - L_t$ and $cos(\pi - x) = -cos(x)$,

$$\begin{aligned}\Omega_{sys} &= \frac{1}{Lsin\left(\frac{\pi}{L}\right)}\left|m^* sin\left(\frac{\pi\left(L_t-\Delta\right)}{L}\right) - sin\left(\frac{\pi\left(L-L_t-\Delta\right)}{L}\right)\right. \\ &\quad \left. + \left(m^*+1\right) sin\left(\frac{\pi\Delta}{L}\right) cos\left(\frac{\pi L_t}{L}\right)\right| \\ &= \frac{sin\left(\frac{\pi(L_t+\Delta)}{L}\right) - m^* sin\left(\frac{\pi(L_t-\Delta)}{L}\right) - \left(m^*+1\right) sin\left(\frac{\pi\Delta}{L}\right) cos\left(\frac{\pi L_t}{L}\right)}{Lsin\left(\frac{\pi}{L}\right)}\end{aligned}$$

Lastly, we twice apply $sin(A+B) = sin(A)cos(B) + sin(B)cos(A)$, find some convenient cancellations, and come to the result quoted in equation (4.12a):

$$\Omega_{sys} = \frac{\left(1-m^*\right) sin\left(\frac{\pi}{2(1-m^*)}\right) cos\left(\frac{\pi\Delta}{L}\right)}{Lsin\left(\frac{\pi}{L}\right)}$$

Comparing with equation (4.12b), we see that the offset adds a factor of $cos\left(\frac{\pi\Delta}{L}\right)$ to Ω_{sys}. Notice that this term is < 1 for all $\Delta > 0$ and monotonically decreasing with Δ for $0 \leq \Delta \leq L/2$, demonstrating that increasing the offset between the clusters in the two lanes always results in a decrease in Ω_{sys}.

B Derivation of Mean-Field Equations of Motion

Here, we derive the mean-field equation for $\partial_t p_0(x)$ (Equation (4.2a)). First, we said that the rate of change of $p_0(x)$ is the rate at which a positive particle moves to the site $(x,0)$ minus the rate at which one moves out of it. We will calculate each by breaking it down into cases.

Positive particles can flow into site $(x,0)$ if two conditions are met: a hole or negative particle occupies the site and a positive particle is in a position to replace it (in site $(x-1,0)$ or $(x,1)$). There are four cases, each with a probability of occurance and a rate at which a switch is made. They are:

Site $(x,0)$	Neighboring Site	Probability	Rate
hole	+ in site $(x-1,0)$	$h_0(x)p_0(x-1)$	1
−	+ in site $(x-1,0)$	$n_0(x)p_0(x-1)$	γ
hole	+ in site $(x,1)$	$h_0(x)p_1(x)$	$1-b$
−	+ in site $(x,1)$	$n_0(x)p_1(x)$	$\gamma(1-b)$

Multiplying the probabilities of each situation existing by the rates of a switch being made, then summing and simplifying yields the total rate at which a positive particle moves to site $(x, 0)$:

$$p_0^{in}(x) = (h_0(x) + \gamma n_0(x))\,(p_0(x-1) + (1-b)p_1(x)) \tag{B.1}$$

Now we turn our attention to the rate at which a positive particle leaves the site $(x, 0)$. As before, we have four cases in which this case occur:

Site $(x, 0)$	Neighboring Site	Probability	Rate
+	hole in site $(x+1, 0)$	$p_0(x)h_0(x+1)$	1
+	− in site $(x+1, 0)$	$p_0(x)n_0(x+1)$	γ
+	hole in site $(x, 1)$	$p_0(x)h_1(x)$	1
+	− in site $(x, 1)$	$p_0(x)n_1(x)$	γ

Again, we multiply probabilities by rates, sum and simplify, to obtain the probability of a positive particle leaving site $(x, 0)$:

$$p_0^{out}(x) = p_0(x)\,(h_0(x+1) + \gamma n_0(x+1) + h_1(x) + \gamma n_1(x)) \tag{B.2}$$

Then to get the total rate at which positive particles move into the site $(x, 0)$, we subtract the flow out from the flow in:

$$\begin{aligned} \partial_t p_0(x) \;=\; & (h_0(x) + \gamma n_0(x))(p_0(x-1) + (1-b)p_1(x)) \\ & - p_0(x)\,(h_0(x+1) + \gamma n_0(x+1) + h_1(x) + \gamma n_1(x)) \end{aligned}$$

This is the result quoted in Equation (4.2a).

C Calculation of α factor for Gatekeeper Generation

Here we calculate the α factor from Section 4.2.1. Recall that, in the three-region structure of the system near transition, there is an offset region where the favored region of lane 1 overlaps the traveler region of lane 0. Also, gatekeepers in lane 0 are generated when a positive particle makes the suppressed exchange with a hole in lane 1 and the two become separated from each other, "trapping" the positive particle in lane 0. The probability that this separation occurs (and thus that the + and hole do not re-exchange) is α. Once the suppressed move is made, the offset region is thus: lane 0 of filled entirely of holes, except for one positive particle, and lane 1 is the opposite, with one hole opposite the positive particle in lane 0, and the remainder full of positive particles. The figure below gives an illustration:

There will also be a few negative particles scattered in lane 1, with an average density of $m^* \approx 0.0256$. We will use notation $(x, 0)$ to refer to the site that contains the positive particle

					+				
+	+	+	+	+		+	+	+	+

in lane 0. In calculating α, we are interested in three moves: (a) the particle at $(x, 0)$ moving right and (b) the particle at $(x-1, 1)$ moving right, which separate the particle and hole at position x, and (c) the particle at $(x, 0)$ moving to lane 1, which "undoes" the cross-lane transition and removes the potential gatekeeper.

When the simulation applies the dynamics to this system, it starts by choosing a particle at random. So the particles at sites $(x, 0)$ and $(x-1, 1)$ are equally likely to be chosen. Then a direction (right, left, or across the lanes) is chosen at random, and a move in that direction is attempted. Note, then, that the three moves we have chosen are equally likely to be attempted. Then α is the ratio of the rates at which (a) or (b) happens before (c).

Suppose that the simulation has selected a bond - call this try 1. We know that in both (b) and (c), the positive particle exchanges with a hole, so the rates from equation (2.1) apply:

$$W_b = W_{phx} = 1 \text{ since } q(x, y) \cdot \delta x = 1 \tag{C.1}$$

$$W_c = W_{phy} = 1 \text{ since } q(x, y) \cdot \delta y = 1 \tag{C.2}$$

There is a small chance, however, that the site $(x+1, 0)$ is occupied by a traveling negative particle. Then combining the occupation densities this site with equation (2.1) reveals that this transition occurs with the rate

$$W_a = (1 - m^*) + m^*\gamma \tag{C.3}$$

Note that there is also a $m^*(1-\gamma)$ probability that the bond in (c) is chosen, but no move is made; in this case, the structure from Figure C remains, and we move to try 2: we choose a particle, then a direction, etc. The probability distribution of (a), (b), and (c) in this case is the same as in try 1. So α is the probability that the particle-hole pair at position x is separated (via either (a) or (b)) divided by the probability that one of the changes ((a) or (b) or (c)) is made. Thus,

$$\alpha = \frac{W_a + W_b}{W_a + W_b + W_c} = \frac{2 - m^*(1-\gamma)}{3 - m^*(1-\gamma)} \tag{C.4}$$

For the high-b value of $m^* = 0.0256$ (measured in Section 3.5 and calculated via equation (4.7)), we obtain $\alpha = 0.6641$.

Vita

Justin August Krometis

Born: July 28, 1980 in Washington, DC

EDUCATION

Virginia Polytechnic Institute and State University, Blacksburg, VA

M.S., Mathematics, 2004
Thesis: *Lane Preference in a Simple Traffic Model*
Advisor: Dr. Beate Schmittmann

B.S., Physics, 2004

B.S., Mathematics, 2002

Glenelg High School, Glenelg, MD, Graduated, 1998

PROFESSIONAL EXPERIENCE

Virginia Polytechnic Institute and State University, Blacksburg, VA

Teaching Assistant
Vector Geometry, Fall 2003-Spring 2004
Elementary Calculus with Matrices, Spring 2003
Calculus Emerging Scholars Program (ESP), Fall 1999

Aurora Biometrics, Vienna, VA, Intern, Summer 2001

Swales Aerospace, Beltsville, MD, Cooperative Education, Spring 2000

NASA Goddard Space Flight Center, Beltsville, MD, Intern, Summers 1997, 1998, 1999

HONORS/AWARDS

H.Y. Loh (Outstanding Senior) Award, Virginia Tech Physics Department, 2004

Outstanding Senior in the Traditional Option, Virginia Tech Math Department, 2002